2016

Analysis of manufacturing parameters on the shear strength of aluminium/GFRP co-cured and adhesively bonded single-lap joints

Reburn, A.

Reburn, A. (2016) 'Analysis of manufacturing parameters on the shear strength of aluminium/GFRP co-cured and adhesively bonded single-lap joints', The Plymouth Student Scientist, 9(2), p. 195-230.
http://hdl.handle.net/10026.1/14133

The Plymouth Student Scientist
University of Plymouth

*The Plymouth Student Scientist, 2016, **9**, (2), 195-230*

Analysis of manufacturing parameters on the shear strength of aluminium/GFRP co-cured and adhesively bonded single-lap joints

Ashley Reburn

Project Advisor: Stephen Grove, School of Marine Science and Engineering, Plymouth University, Drake Circus, Plymouth, PL4 8AA

Abstract

Due to the increased application of composite materials in recent years, the process of joining composites to metals has become a key area of interest. As a result, methods to increase the strength of composite-to-metal joints are highly sought after. Since the mechanical behaviour of composite-to-metal joints depends on many manufacturing parameters. An experimental and numerical study into the shear strength behaviour of GFRP-to-aluminium single-lap joints was performed to investigate the effect of four manufacturing parameters, with the aim of optimising shear strength. For one manufacturing parameter, a relatively new joining process, co-curing, is studied, and results are benchmarked against secondary (adhesively) bonded joints. The results of this study provides a better understanding of the co-curing process which will increase the application of co-curing in industry. From the results, an increase in adherend (or substrate) thickness and surface roughness were found to increase joint strength. For certain manufacturing configurations, co-cured joints were similar in strength to adhesively bonded ones. The failure mechanism of the co-cured and adhesively bonded single-lap joints was discussed using stress distributions obtained from finite element analysis (FEA) and fractography. It was found that the failure mechanism of co-cured lap joints was cohesive failure by delamination at the first ply layer of the composite adherend. Adhesively bonded joints failed by a mixture of cohesive failure with peel. Results of this study present how the co-cured joining method can be regarded as a highly efficient manufacturing process, which can be tailored to match the strength of traditional joining methods.

Nomenclature

Abbreviation	Description	Units
ANOVA	Analysis of Variance	n/a
CLSM	Confocal Laser Scanning Microscope	n/a
FEA	Finite Element Analysis	n/a
FEM	Finite Element Model	n/a
FRP	Fibre-Reinforced Plastic	n/a
GFRP	Glass Fibre Reinforced Polymer	n/a
MDF	Medium-density Fibreboard	n/a
SEM	Scanning Electron Microscope	n/a
SPC	Statistical Process Control	n/a
UTM	Universal Test Machine	n/a
$\bar{x}$	Mean	n/a
XRF	X-ray Fluorescence	n/a
Symbol	**Description**	**Units**
A	Shear Area	mm^2
F_{max}	Failure Load	N
SR_a	Arithmetic Average	µm
SR_p	Maximum Peak Height	µm
SR_q	Root Mean Squared	µm
SR_v	Maximum Valley Depth	µm
SR_z	Average Distance between Highest Peak and Lowest Valley	µm
t_a	Adherend Thickness	mm
t_b	Bondline Thickness	mm
τ_{xy}	Tensile Lap-shear Strength	MPa

Introduction

The traditional joining methods for composite-to-metal structures are generally classified into mechanical joining, and, combined mechanical and secondary (adhesive) bonding. Mechanical joints are suitable where disassembly is required, however the downsides of this joining process are an increase in mass and the presence of stress concentrations. In the case of fibre-reinforced plastic (FRP) structures, the drilling process can damage reinforcement fibres within the composite part, which can initiate fatigue cracks (Matsuzaki *et al*. 2008a). There are widespread advantages of adhesively bonded joints in comparison to traditional joining methods. Benefits include, weight savings and more importantly damage tolerance (O'Mahoney *et al*. 2013). This property is common within the aerospace industry, and as a result, the application of adhesive bonding has been mainly directed towards this sector in recent years. Typical applications within the aircraft industry include, bonding stringers to skins in wings and fuselages (O'Mahoney *et al*. 2013). These materials may be either metallic or composite, and with the increased use of composite materials in the aircraft, marine and automotive industry, composite-to-metal bonding is a key area of interest.

Since adhesive bonding is sensitive to manufacturing parameters, better bonding techniques are required, whereby quality can be built into the manufacturing process and the reliability improved to match traditional joining methods. Thus, co-curing has been developed which is regarded as an adhesive bonding process (Wahab, 2015). From a manufacturing perspective, co-curing is highly efficient because both curing and joining of the composite structure can be achieved simultaneously. The process requires neither an adhesive nor surface pre-treatment of the composite part, because excess resin, which is extracted from the composite material during consolidation is used in the bonding process (Wahab, 2015). From a design viewpoint, since the adhesive of the co-cured joint is the same material as the resin of the composite part, the analysis and design of co-cured joints are simpler than adhesively bonded ones (Shin *et al*. 2003). Despite these advantages, only a few related studies on the co-cured joining method are available (Shin *et al*. 2003; Kwang-Soo Kima, 2006; Seong *et al*. 2008; Matsuzaki *et al*. 2008a; Matsuzaki *et al*. 2008b; Tzetzis, 2012).

The structural performance of bonded joints depends on many variables, mainly, adherend (substrate) thickness, adhesive layer (bondline) thickness, overlap length and surface preparation. Although many numerical and experimental investigations have been conducted for these parameters, the influence of adherend thickness on the static behaviour in co-cured GFRP-to-aluminium single-lap joints has not yet been studied. In the many studies on co-cured single-lap joints, much of the work is focused around surface pre-treatment and surface roughness (Kwang-Soo Kima, 2006; Tzetzis, 2012).

Although a reduction in labour and manufacturing costs are possible from the co-curing process, a substantial increase in joint strength compared with adhesive bonding cannot be expected (Matsuzaki *et al*. 2008b). Therefore, methods to increase the strength of co-cured joints are highly sought after.

In this work, a numerical and experimental study was conducted to investigate the influence of four manufacturing parameters (adherend thickness, bondline thickness, bonding process and surface preparation) on the shear behaviour of GFRP-to-

aluminium single-lap joints under static tensile loading. Experimental testing was conducted in accordance with ASTM D5868 - 01 (ASTM International, 2014). The purpose of the finite element model (FEM) was to study stress distributions along the overlap region, which cannot be obtained through experimental investigation.

In order to understand the effect of each manufacturing parameter, a full manufacturing analysis was conducted by statistical hypothesis testing in MATLAB R2015b (The MathWorks Inc, 2016). It is hoped that these results, will enable engineers to optimise the shear strength of co-cured joints, so that the manufacturing process is applicable to industrial applications. Finally, fracture surfaces for each manufacturing process were examined by scanning electron microscopy (SEM), and failure modes characterised in accordance with BS EN ISO 10365 (British Standards Institution, 1995).

Materials and experimental details

In this study, composite adherends were fabricated using a 0/90° woven E-glass fibre-epoxy laminate. The metallic adherend is a 1000 series 1050 H19 aluminium alloy. Adhesively bonded joints were assembled using a two-component epoxy structural adhesive (Spabond 340LV) from Gurit (Gurit , 2016). Co-cured joints were fabricated using a two-component resin infusion epoxy system (SR 8100/SD 8824) from Sicomin (Sicomin Epoxy Systems, 2016). The chemical composition of the metallic adherend obtained by X-ray fluorescence (XRF) analysis using an Olympus XRF analyser (OLYMPUS CORPORATION, 2016) is shown in Table 1. Material properties are presented in Appendix B.

Table 1: Chemical composition of 1050 H19 aluminium alloy adherend, obtained by XRF analysis.

Element	Al	Cu	Fe	Mn	Si	Ti	V	Zn
Weight [%]	99.52	0	0.33	0	0.15	0	0	0

For both the co-cured and adhesively bonded test specimens, 1.5mm by 25.4mm by 101.6mm flat aluminium coupons were cut to length. Prior to bonding, contacting surfaces were de-greased and scarified by abrading with a dry P80 grit paper in accordance with BS EN 13887:2003 to achieve uniform and consistent scarification. After debris removal using compressed air, abraded surfaces were finally cleaned with acetone solvent prior to bonding to eliminate surface contamination and promote adhesion. During this study, additional testing was conducted to evaluate the influence of surface pre-treatment for either bonding process. Specimens prepared by mechanical blasting were de-greased and then dry blasted with alumina grit in accordance with BS EN 13887:2003, and bonded immediately after debris removal and cleaning.

In single-lap joints under tensile loading, shear and out-of-plane loads (peel stresses) occur and are a maximum at the free ends of the overlap region due to the geometry of the lap joint which generates bending moments (Kinloch, 1987). To minimise these effects, the geometry of the single-lap joints uses end-tabs as shown in Figures 1 and 2 so that the applied force will be in-plane.

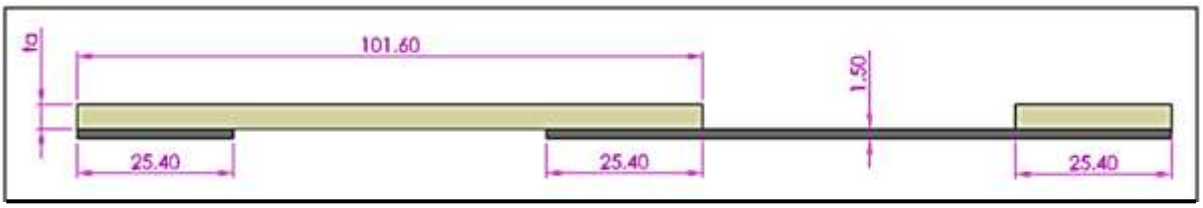

Figure 1: Specimen configuration of the co-cured single-lap joints. *(not to scale, dimensions in mm)*

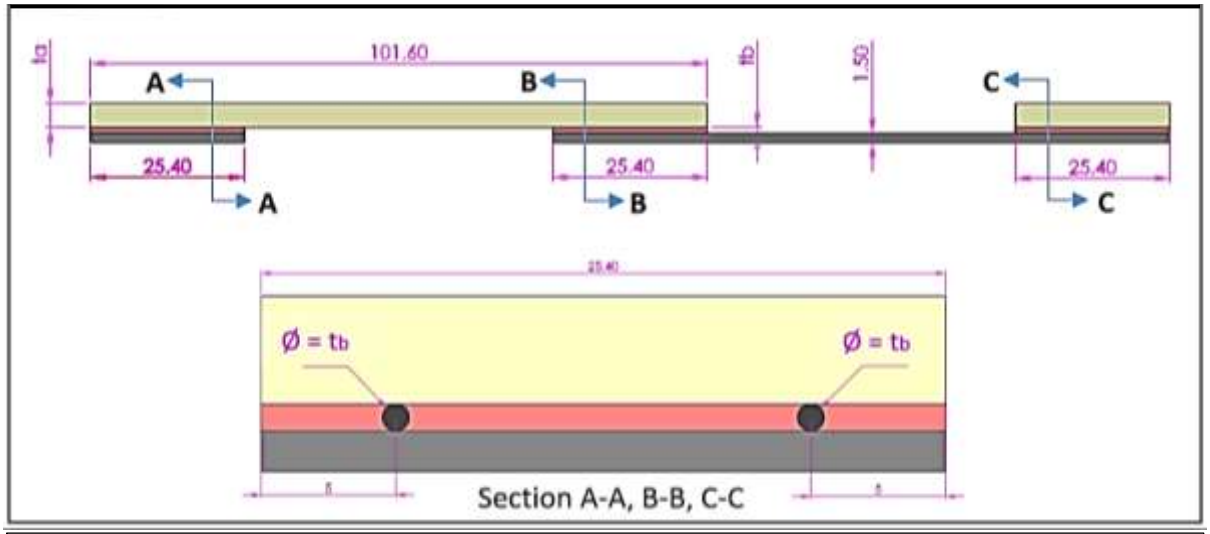

Figure 2: Specimen configuration of the adhesively bonded single-lap joints. Section view showing the cross-sectional geometry at region A-A, B-B and C-C, picturing the calibrated aluminium wire spacers which were used to control bondline thickness. *(not to scale, dimensions in mm)*

During this study, co-cured specimens are benchmarked against adhesively bonded joints which are more preferred but still less widely used in industry (Wahab, 2015). The effect of composite adherend thickness (t_a) was analysed by considering a laminate composed of 10, 15 and 20 plies. For the adhesively bonded joints, three separate bondline thicknesses, t_b, (0.56, 0.76 and 1.00 mm) were examined and controlled using calibrated aluminium wire spacers (see Figure 2). A bondline thickness of 0.76mm was selected as a benchmark for comparison between the two bonding processes, as this is consistent with ASTM D5868 – 01. Lastly, the effect of two different surface pre-treatments; mechanical abrasion and mechanical blasting are considered. Table 2 summarises the manufacturing parameters and specimen labels used in this study.

Table 2: Specimen labels and manufacturing details.

Test Number	Sample	Bonding Process	Surface Preparation	Substrate A Thickness, t_a	Bondline Thickness, t_b (mm)	Number of Specimens
1	A	Co-Cured	Mechanical Abrasion	20 Plies	-	8
2	B	Co-Cured	Mechanical Abrasion	15 Plies	-	8
3	C	Co-Cured	Mechanical Abrasion	10 Plies	-	8
4	D1	Adhesive	Mechanical Abrasion	20 Plies	0.56	10
5	D2	Adhesive	Mechanical Abrasion	20 Plies	0.76 (ASTM D5868 - 01)	10
6	D3	Adhesive	Mechanical Abrasion	20 Plies	1	10
7	E1	Adhesive	Mechanical Abrasion	15 Plies	0.56	10
8	E2	Adhesive	Mechanical Abrasion	15 Plies	0.76 (ASTM D5868 - 01)	10
9	E3	Adhesive	Mechanical Abrasion	15 Plies	1	10
10	F1	Adhesive	Mechanical Abrasion	10 Plies	0.56	10
11	F2	Adhesive	Mechanical Abrasion	10 Plies	0.76 (ASTM D5868 - 01)	10
12	F3	Adhesive	Mechanical Abrasion	10 Plies	1	10
13	G1	Adhesive	Mechanical Blasting	10 Plies	0.76	10
14	G2	Co-Cured	Mechanical Blasting	10 Plies	-	8
					Total	**132**

The application of the proposed joints is typically aerospace, marine and automotive applications where aluminium and GFRP are often used. Thus, a chemical pre-treatment was not applied to the aluminium contacting surface, since this would not be feasible for the vast majority of industrial applications. Instead, abrasive surface treatments were adopted. In total, 132 single-lap joint specimens were fabricated and tested according to 14 different variations.

For each test specimen, static tensile tests were performed in accordance with ASTM D5868 – 01. Specimens were tested to failure and corresponding failure modes for each bonding process were examined by a SEM. The thickness of the aluminium adherends (1.5mm) and overlap length (25.4mm) were consistent throughout the course of this study. Tensile tests were carried out using an Instron 5582 screw-driven 100kN universal test machine (UTM) with self-aligning grips (Instron, 2016), and performed at a constant cross-head speed of 13mm/min. For each test condition a minimum of eight specimens were tested. Figure 3 shows the typical failure sequence during testing.

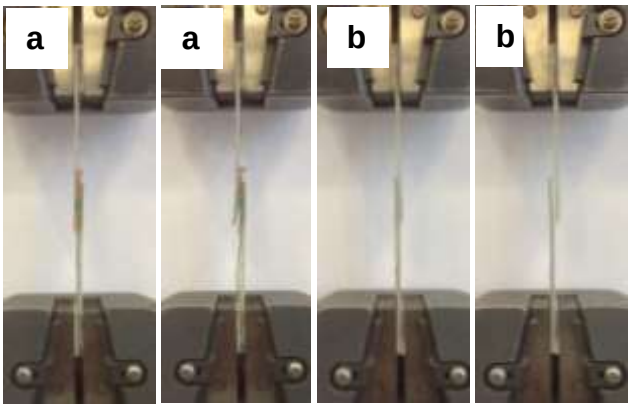

Figure 3: Typical failure sequence during static tensile testing for; (a) adhesively bonded and (b) co-cured single-lap joints.

Adhesively bonded single-lap joints

Composite adherends of the adhesively bonded joints were fabricated by vacuum resin infusion and cut into flat coupons using a diamond tip water-cooled circular saw. After debris removal using compressed air, composite adherends were finally degreased and cleaned using acetone prior to bonding. Bonded contacting surfaces of the composite adherends utilised the surface texture generated from the peel ply during the infusion process. To achieve consistent bonding, specimens were assembled using a wooden medium-density fibreboard (MDF) adhesive bonding jig pictured in Figure 4. The use of a jig ensures accurate alignment of the adherends and that the correct overlap length is maintained. Additionally, the jig allows for bondline thickness control by insertion of calibrated aluminium wire spacers, which were aligned parallel to the direction of loading as this minimises the effect of the wire on the shear behaviour of the joint. Specimens were finally compressed with a uniform and constant applied pressure for the entire cure cycle.

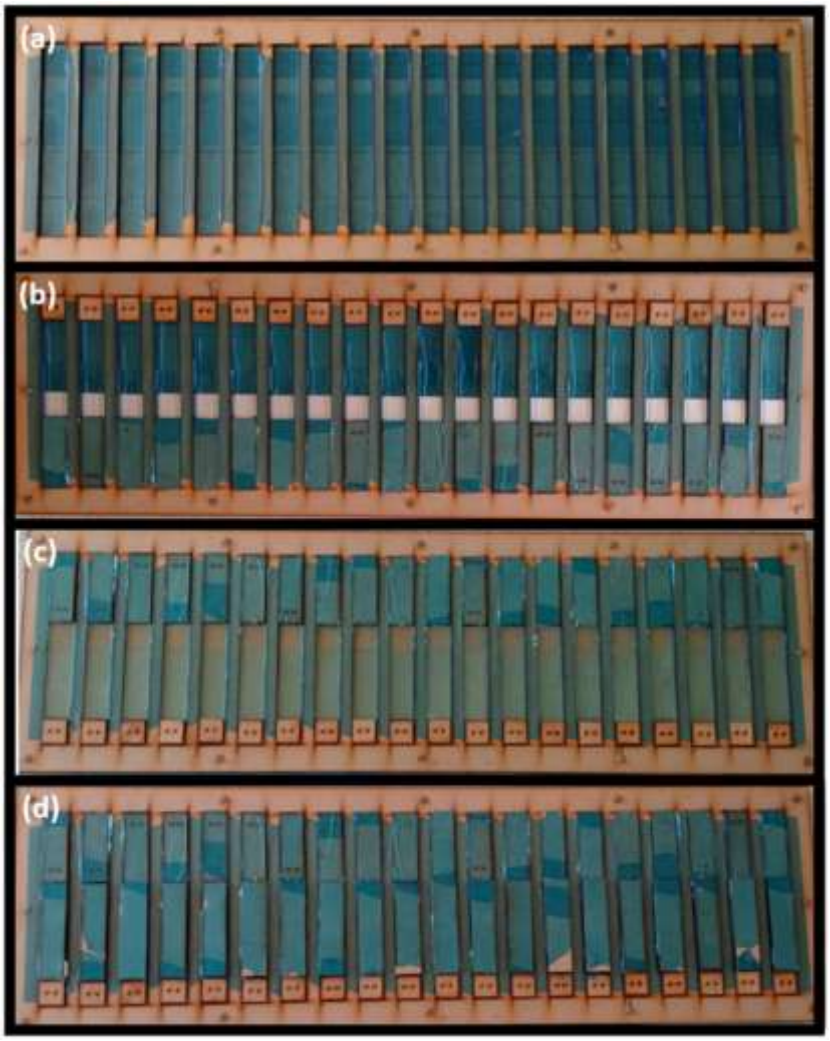

Figure 4: MDF adhesive bonding jig, showing the four stages in assembly preparation; (a) release film application, (b) insertion of calibrated wire spacers and setup of overlap length control, (c) adhesive application and bonding, (d) clamping.

Co-cured single-lap joints

Co-cured specimens were fabricated by overlapping dry glass fibre reinforcement over surface pre-treated aluminium adherends prior to vacuum resin infusion. A stopper was used to control overlap length, and layup of reinforcement fibres was carried out parallel with the contacting surface of the aluminium adherend. The infusion resin was the same two-component epoxy system utilised for fabricating the GFRP adherends of the adhesively bonded joints. During infusion, epoxy resin is impregnated into the reinforcement fibres under vacuum, and specimens were cured under atmospheric pressure and at room temperature for 24 hours. During consolidation, the GFRP laminate is simultaneously bonded to the aluminium adherends. Polymer spacers between the aluminium adherends were used during the fabrication process (see Figure 5), which provides spacing to allow specimens to be cut to the required geometry using a diamond tip water-cooled circular saw. Finally, end-tabs were bonded to either adherend using dissimilar materials. An elevated cure was not selected for either bonding process as this would not be practical for most industrial applications. Similarly, since there is a difference in the coefficient of thermal expansion between the aluminium and composite adherend, an elevated cure would induce thermal residual stresses and this could impart bond strength. Figure 6 shows a typical fabricated specimen for either bonding process.

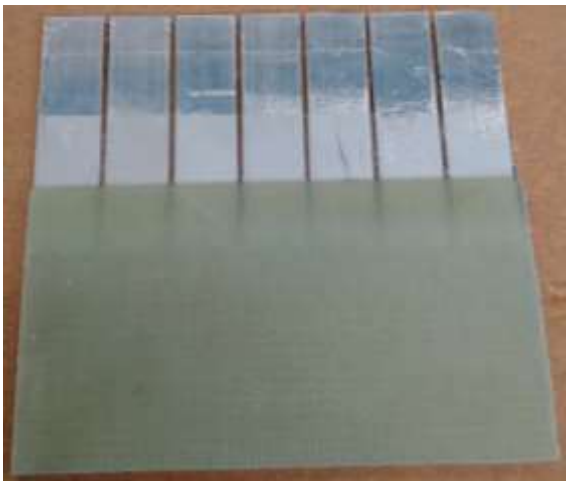

Figure 5: Co-cured test plate prior to cutting, showing the 2 mm polymer spacers separating the aluminium adherends.

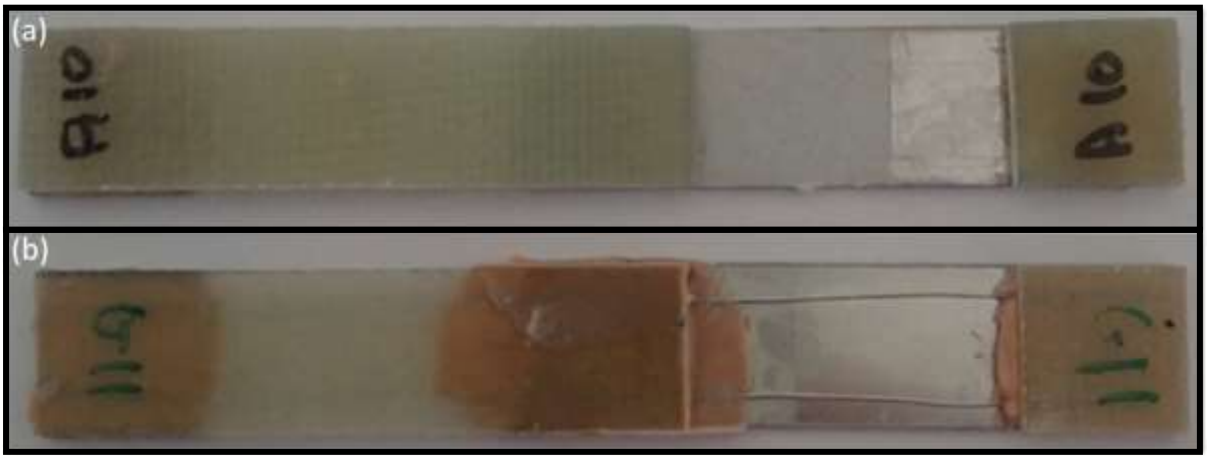

Figure 6: Typical fabricated specimens; (a) co-cured and (b) adhesively bonded single-lap joint.

Statistical methodology

Processing of all raw data and comparative statistical analysis was conducted using MATLAB R2015b from MathWorks (The MathWorks Inc, 2016). For each test specimen, the failure load was obtained by recording the highest load during testing. A typical load-extension graph is shown in Appendix D. Test specimens that failed through adherend failure were discarded from the statistical analysis. The tensile lap-shear strength, τ_{xy}, in mega-pascals (MPa), is calculated by dividing the breaking force, F_{max}, in newton's (N), by the shear area, A, in square millimetres (mm²) as shown in Equation 3.1. For the adhesively bonded test specimens, the loss in shear area as a result of the wire spacers is considered in these calculations.

$$\tau_{xy} = \frac{F_{max}}{A} \qquad \textbf{Eq. 3.1}$$

Prior to comparative statistical analysis, winsorizing of raw data was conducted by means of Lilliefors normal distribution tests, two-sample F-tests for equal variance and mean testing using two-sample t-tests. These tests compare the normality, variance and means between the original and winsorized data. For each test presented in this study, a result of h=1 rejects the null hypothesis at the 1% significance level, and 0 otherwise. From these results, any noticeable outliers were identified and eliminated from the forthcoming analysis. Appendix F summarises the results of this analysis. Table 3 below, summarises all comparative statistical tests examined in this study.

Table 3: Statistical analysis combination table.

Test Number	Sample Combination			Independent Variable	Comparison Parameters		
	Sample 1	Sample 2	Sample 3		Sample 1	Sample 2	Sample 3
1	A	D2	-	Bonding Process	Co-Cured	Adhesive	-
2	B	E2	-	Bonding Process	Co-Cured	Adhesive	-
3	C	F2	-	Bonding Process	Co-Cured	Adhesive	-
4	G1	G2	-	Bonding Process	Adhesive	Co-Cured	-
5	G1	F2	-	Surface Preparation	Mechanical Blasting	Mechanical Abrasion	-
6	G2	C	-	Surface Preparation	Mechanical Blasting	Mechanical Abrasion	-
7	A	B	C	Substrate A Thickness	20 Plies	15 Plies	10 Plies
8	D2	E2	F2	Substrate A Thickness	20 Plies	15 Plies	10 Plies
9	D1	D2	D3	Bondline Thickness (mm)	0.56	0.76	1
10	E1	E2	E3	Bondline Thickness (mm)	0.56	0.76	1
11	F1	F2	F3	Bondline Thickness (mm)	0.56	0.76	1

For statistical analysis 1 to 6 (two-sample testing) shown in Table 3, comparative statistical analysis was conducted by means of equal variance two-sample t-tests. This determines whether the difference between sample means or joint strengths are significant. For the tests involving populations with unequal variance, unequal variance two-sample t-tests were conducted. For further validation, log transformation testing was conducted which improves the stability and linearity of the populations by reducing skewness, this additionally eliminates any bias from the analysis. Non-parametric Kruskal-Wallis tests were also performed to assess one-way analysis of variance (ANOVA). Results of this analysis are presented in Appendix G.

For statistical analysis 7 to 11 (three-sample testing) shown in Table 3, comparative statistical analysis was conducted by means of one-way ANOVA. For each analysis,

Bartlett's test for homogeneity of variances (homoscedastic) was conducted to estimate whether more than two groups are homoscedastic.

After which, multiple comparison mean testing was conducted in order to determine which samples are significantly different, as performing multiple two-sample t-tests to determine which pairs of means are significantly different would be highly inefficient. Confidence interval graphical plots were used to validate these results. Results are presented in Appendix H, see Appendix E and K for a detailed statistical methodology and test statistics.

Numerical analysis

Modelling approach

A numerical study was performed in order to better understand the effect of composite adherend thickness on the out-of-plane tensile (peel) and shear stress distributions at the first ply of the composite adherend and within the adhesive layer. Keeping with experimental data, three adherend thicknesses (10, 15 and 20 plies) were considered. For the adhesively bonded joints, a bondline thickness of 0.76mm was modelled neglecting the aluminium wire spacers used in experimental testing. For the co-cured joints, 1.5mm radius fillets that are generated during the fabrication process were incorporated into the model.

For both bonding processes, composite adherends were modelled using an orthotropic linear-elastic material. Aluminium adherends and the bulk adhesive were modelled using a linear-elastic isotropic material. Material properties for the aluminium adherend and bulk adhesive were obtained from CES EduPack (GRANTA DESIGN, 2015). For the composite adherend, material properties were obtained from Autodesk Simulation Composite Design (Autodesk Inc, 2016). The thickness of each lamina is 0.2126mm. Material properties are shown in Appendix B.

A three-dimensional FEM was developed, and solved using SolidWorks Simulation finite element code (Dassault Systèmes SolidWorks Corp, 2015). A typical meshed three-dimensional model is shown in Figure 7.

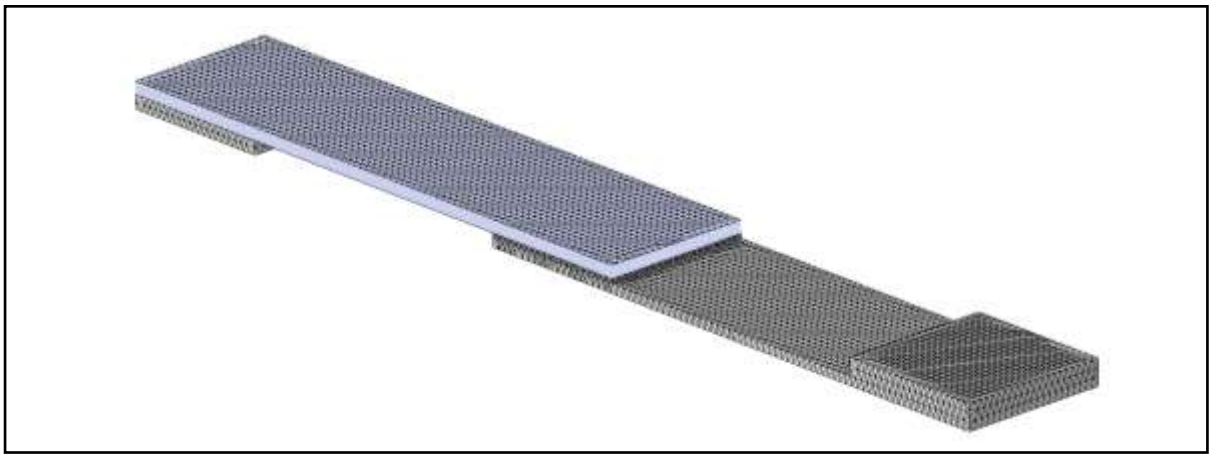

Figure 7: Typical meshed three-dimensional model.

A finer mesh was used within the overlap region, in particular along the free edges and corner regions. The two contacting surfaces within the adhesively bonded joints were modelled using bonded contact connections. Co-cured joints, were assumed to be perfectly bonded at the interface between the composite and aluminium adherend (Shin *et al*. 2003), consequently the microscopic adhesive layer was ignored in the analysis. Figure 8 shows typical boundary conditions and models of the co-cured and adhesively bonded joints. For each analysis, a uniform tensile load of 1500N was applied.

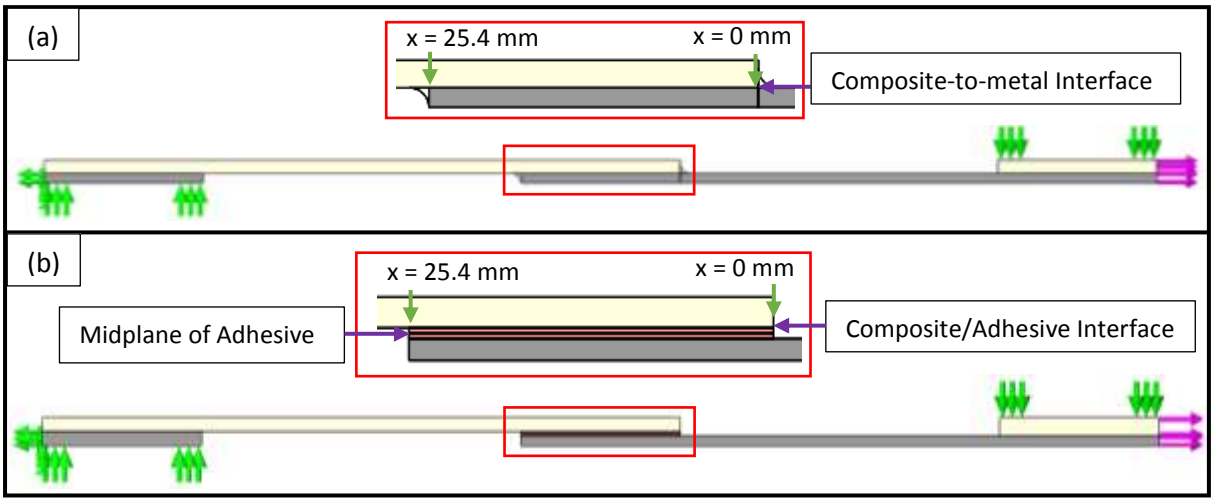

Figure 8: Typical boundary conditions for; (a) co-cured and (b) adhesively bonded single-lap joints. X-distance refers to the results presented in Figure 9.

Results presented in Figure 9, 1a to 1c, illustrate how shear stresses are non-uniformly distributed, and concentrated at the ends of the overlap region due to eccentricity and differential straining of the substrates (Kinloch, 1987). This is in good agreement with Volkersen's shear-lag analysis (Volkersen, 1938). In graphical plots 1a and 1c, shear stresses trend towards a zero shear stress condition at the end of the composite adherend, as expected (Kinloch, 1987; Zhao *et al*. 2011). For the adhesively bonded joints, peak stresses decrease with a corresponding increase in adherend thickness, this is more distinctive at the end of the aluminium adherend (x=25.4mm). More uniform stress distribution occurs due to a larger ratio between the stiffness of the composite adherend and the adhesive layer, therefore less elastic deformation of the joint occurs.

For the co-cured joints (1c), a directional change in shear stresses is found near the free end of the composite adherend (x=0mm), as a consequence of interlaminar shear stresses within the composite adherend. Later on in this study, the interlaminar shear strength of the composite adherend is found to be a leading factor in the failure of the co-cured specimens. Peel stresses presented in Figure 9, 2a to 2c, show a similar effect and peak stresses near the free ends are reduced with a corresponding increase in adherend thickness. This is expected since the rigidity of the joint increases, less elastic deformation occurs, and consequently lower stress concentrations at the free ends of the overlap region occur which supposedly increases joint strength (Reis *et al.* 2011).

Numerical Results

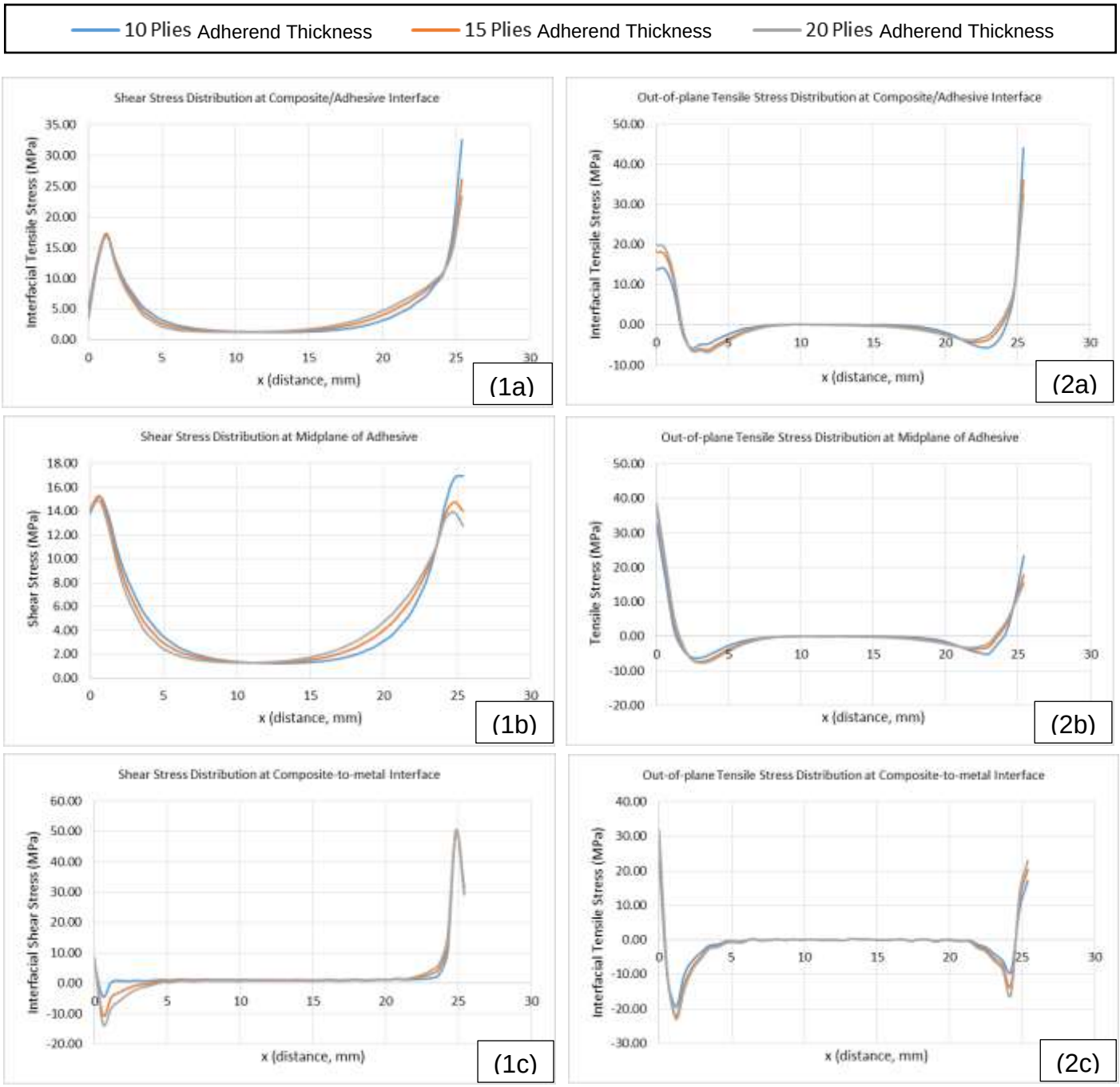

Figure 9: Numerical results for shear (1) and out-of-plane tensile (2) stress distributions. For adhesively bonded joints, stress distributions were obtained at (a) the composite-adhesive interface and (b) along the midplane of the adhesive layer. For co-cured joints (c), results were obtained at the composite-to-metal interface.

At the free end of the composite adherend, peel stresses are magnified and this can be explained by an increase in bending moments which constitutes to yielding of the aluminium adherend. Furthermore, contacting surfaces near the free ends of the overlap region are put into compression as a result of joint rotation.

The results of this analysis agree with the numerical studies conducted by Goland and Reissner (1944), Pereira *et al*. (2010), Reis *et al*. (2011) and Pinto *et al.* (2014). For the adhesively bonded joints, the stress distributions are more uniformly distributed, and consequently higher joint strengths are obtained. In the co-cured joints, increasing the thickness of a single adherend results in peel and shear stresses concentrated at one end of the joint, this results in less uniform distribution of stresses and hence lower joint strengths.

Experimental Results

Fractography study

Figure 10 shows photographs of a typical pair of failure surfaces from the co-cured and adhesively bonded samples. On visual inspection, initial failure mechanism of the adhesively bonded joints depicts a mixture of cohesive failure with peel. This mode of failure is characterised by rupture of the bonded assembly in which the separation appears visually to be in the adhesive (British Standards Institution, 1995). For each fractured specimen there was noticeably more adhesive located at the free end of the aluminium adherend. As a consequence of loading eccentricity, small pockets of adhesive are pulled away from the GFRP adherend during fracture. The influence of shear stresses was noticeable along the longitudinal edges of each test specimen where cohesive failure was most dominant.

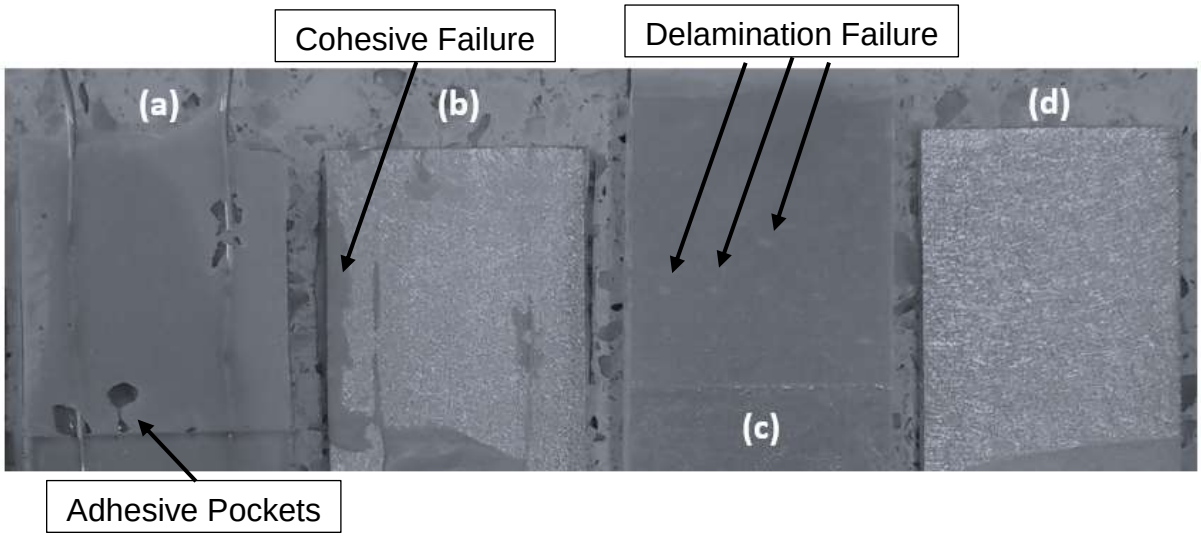

Figure 10: Photograph showing the typical failure surfaces obtained from tensile testing. (a) GFRP adherend, and (b) aluminium adherend of adhesively bonded single-lap joint; (c) GFRP adherend, and (d) aluminium adherend of co-cured single-lap joint.

On visual inspection, there was no clear indication of cohesive failure within the co-cured specimens. Consequently, it was difficult to distinguish which mode of adhesive failure had occurred. On the failure surface of the composite adherend, delamination failure was clearly visible due to the presence of glass fibres exposed at the surface. For clarification, more detailed investigations into the failure surface topography were conducted using a SEM. For analysis, fracture surfaces were cut to a suitable size and mounted rigidly on a specimen stub using copper tape. Finally specimens were coated in gold (see Figure 11) by a K550X low-vacuum sputter coater from Quorum Technologies (Quorum Technologies, 2016) and then analysed under a high-pressure vacuum using a JSM-6610 Series SEM from JEOL (JEOL , 2016).

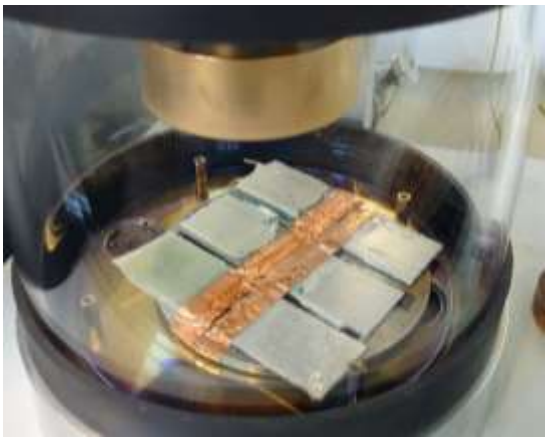

Figure 11: Showing the typical fracture surfaces mounted on a specimen stub prior to low-vacuum sputter coating.

Figure 12 shows the typical fracture surfaces of an adhesively bonded test specimen observed under SEM. In this figure, micrographs 1 to 8 confirm the initial observations made by visual inspection. From the micrographs, it is clear that a large number of air cavities are present throughout the adhesive layer, and this almost inevitably influences the shear strength of the joint. Fracture planes are clearly visible within micrographs 1 and 2 under the action of shear stresses within the adhesive layer, and this fracture surface is typical of cohesive failure (British Standards Institution, 1995). Note that micrographs 5 and 6 are the corresponding fracture surfaces of micrographs 1 and 2, and corresponding fracture planes are found. It is clear from micrograph 3 that peel stresses are present at the free ends of the overlap region. Although peel stresses have been minimised through the adoption of end-tabs; peel stresses are inevitable due to the geometry of the single-lap joint which introduces loading eccentricity. Bending stresses promote peel at both ends of the overlap region which creates pockets in the adhesive layer as pictured in micrograph 4. Micrograph 7 is the matching fracture surface of micrograph 4, and shows how the adhesive material remains firmly bonded to the aluminium adherend. Notice that in micrograph 8, the adhesive is abundant at the free edge and progressively decreases in the longitudinal direction. This fracture surface is typical of cohesive failure with peel (British Standards Institution, 1995). Thus, in certain regions, adhesion to the metal and composite surface is stronger than the strength of the adhesive itself.

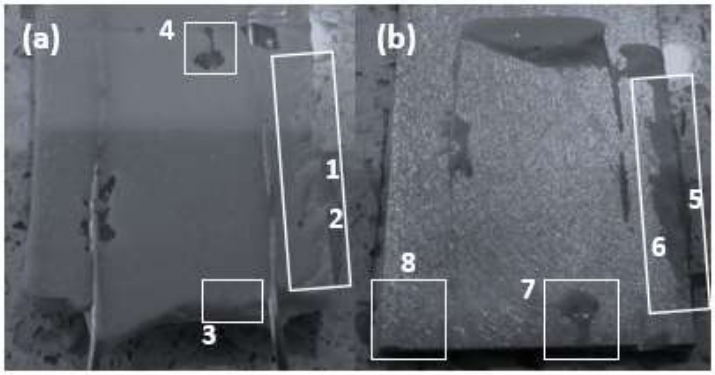
(a)
4
1
2
3
(b)
5
6
8
7

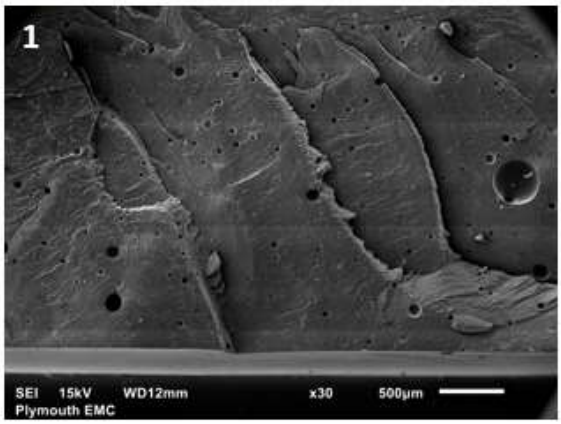
1
SEI 15kV WD12mm x30 500µm
Plymouth EMC

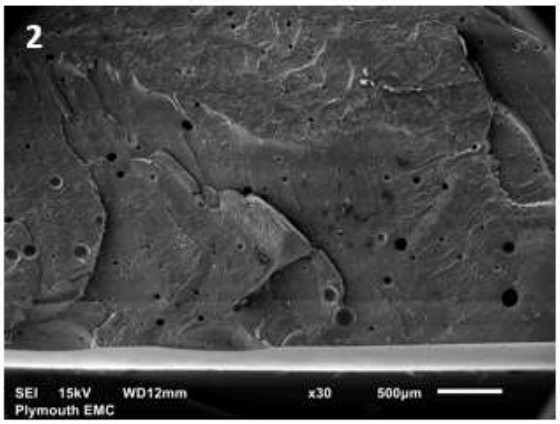
2
SEI 15kV WD12mm x30 500µm
Plymouth EMC

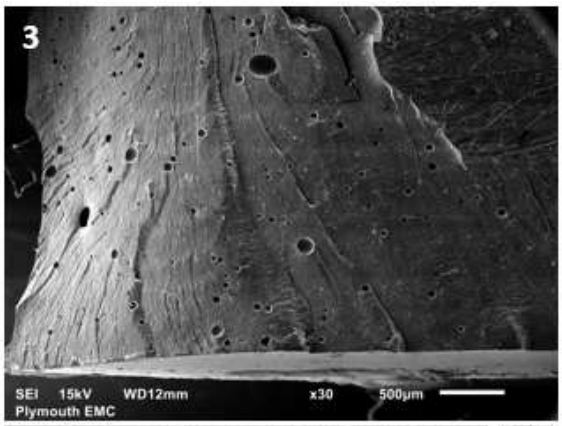
3
SEI 15kV WD12mm x30 500µm
Plymouth EMC

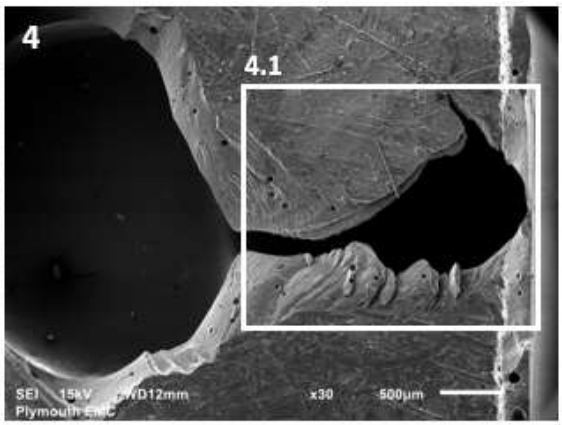
4
4.1
SEI 15kV WD12mm x30 500µm
Plymouth EMC

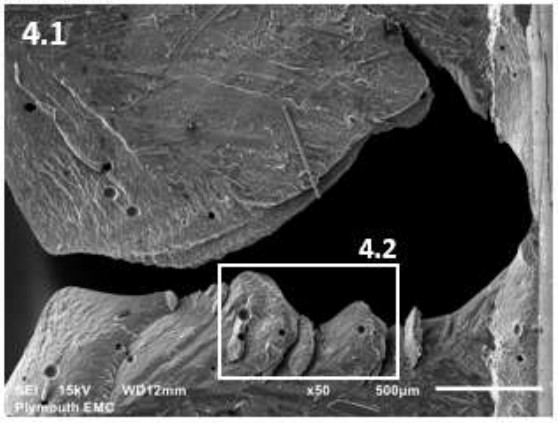
4.1
4.2
SEI 15kV WD12mm x50 500µm
Plymouth EMC

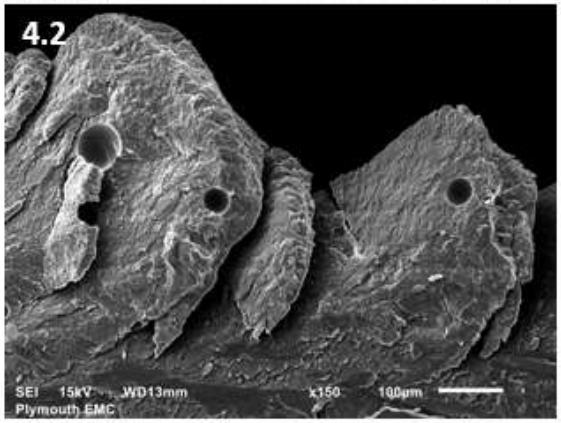
4.2
SEI 15kV WD13mm x150 100µm
Plymouth EMC

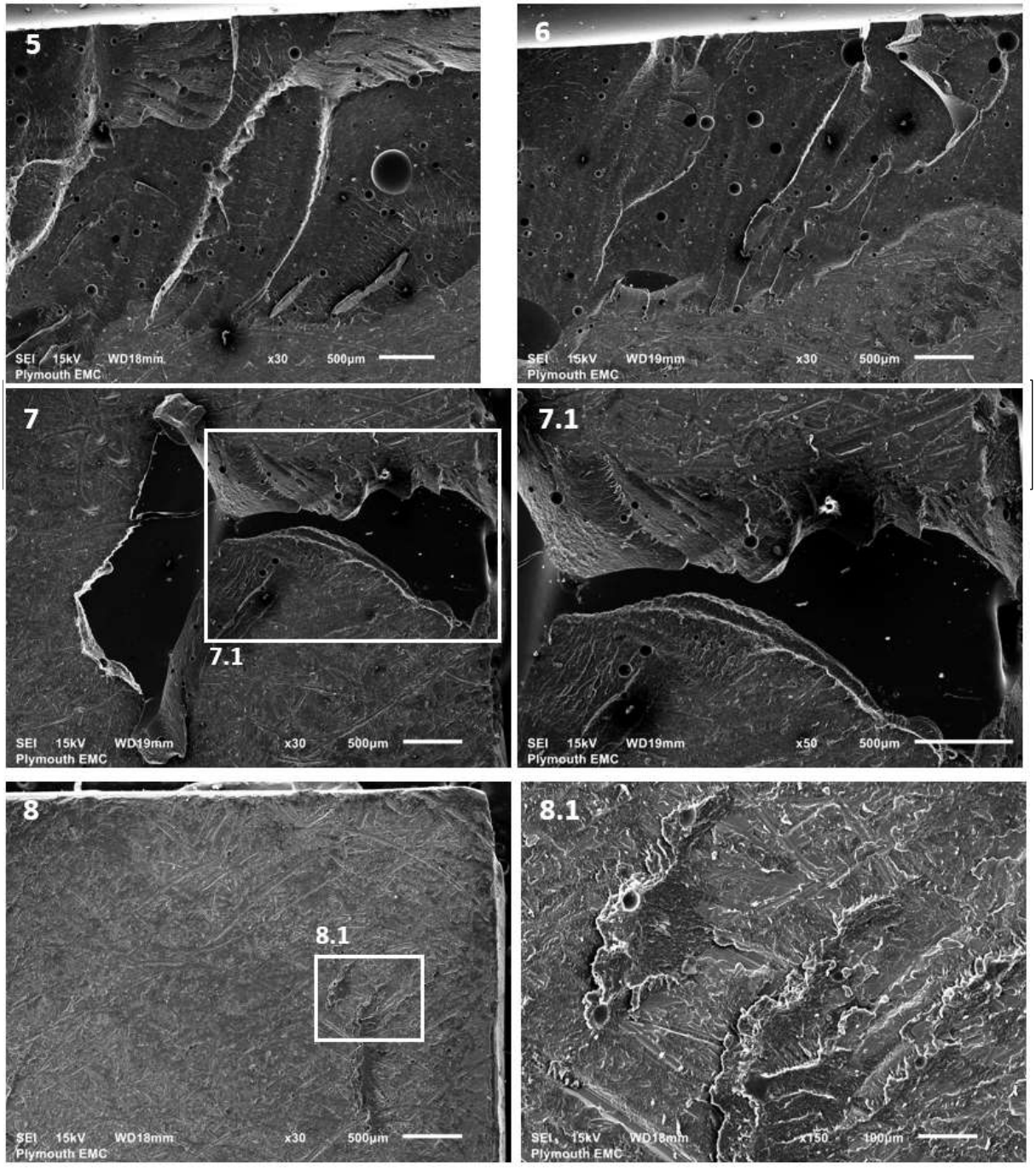

Figure 12: Photograph and micrographs showing the typical fracture surface of an adhesively bonded single-lap joint observed under SEM. (a) fracture surface of GFRP adherend; (b) fracture surface of aluminium adherend.

Figure 13 shows the typical failure surfaces of a co-cured test specimen analysed under SEM. The first observation is that the adhesive layer shows no sign of air cavities unlike the adhesively bonded specimens. In micrographs 9 and 10, resin is pulled away from the GFRP adherend under the shear and peeling action of the

aluminium adherend. This leaves behind pockets in the first ply layer, exposing glass fibres in the second ply layer. Resin that is pulled away from the composite adherend remains firmly bonded to the aluminium adherend as shown in micrographs 13.

In the co-cured specimens, the failure mechanism was shown to be cohesive failure by delamination at the first ply of the composite adherend, as shown in micrographs 9, 10 and 11. This indicates that adhesion between the composite and metal substrate is stronger than the interlaminar shear strength of the composite adherend (Kwang-Soo Kima, 2006). This highlights a key area in the development of co-cured joints, and suggests that improvements in joint strength can be obtained by modifying the composite stacking sequence to increase interlaminar shear strength of the composite part.

In micrograph 12.1, it is interesting how along the longitudinal edges of the overlap region the joint exhibits a similar failure mode to the specimens observed in micrographs 1 and 2 for the adhesively bonded joints. Fracture planes, are clearly visible under the action of shear stresses within the adhesive layer. At the free end of the composite adherend, peel stresses introduce a small degree of fibre breakout (micrograph 12.2). The results of this analysis confirm that the failure mode of co-cured joints is typical of a cohesive failure with peel and delamination at the first ply.

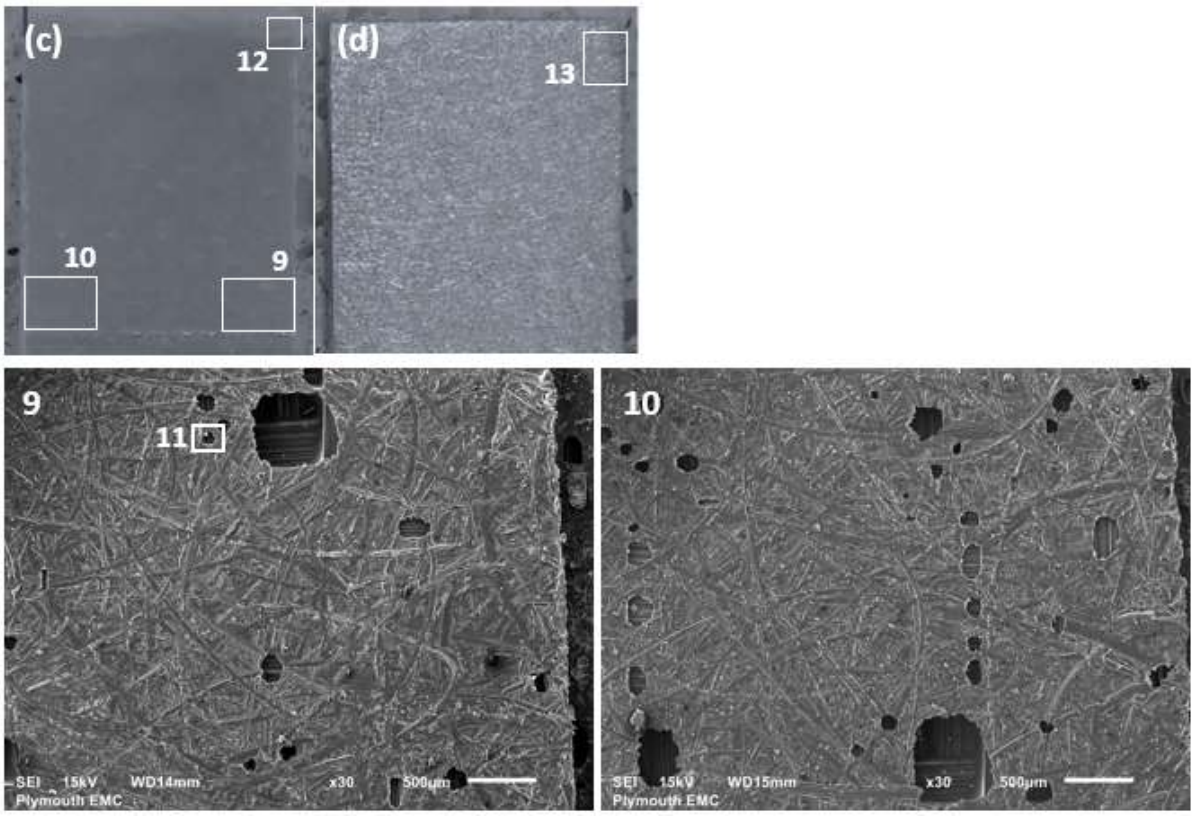

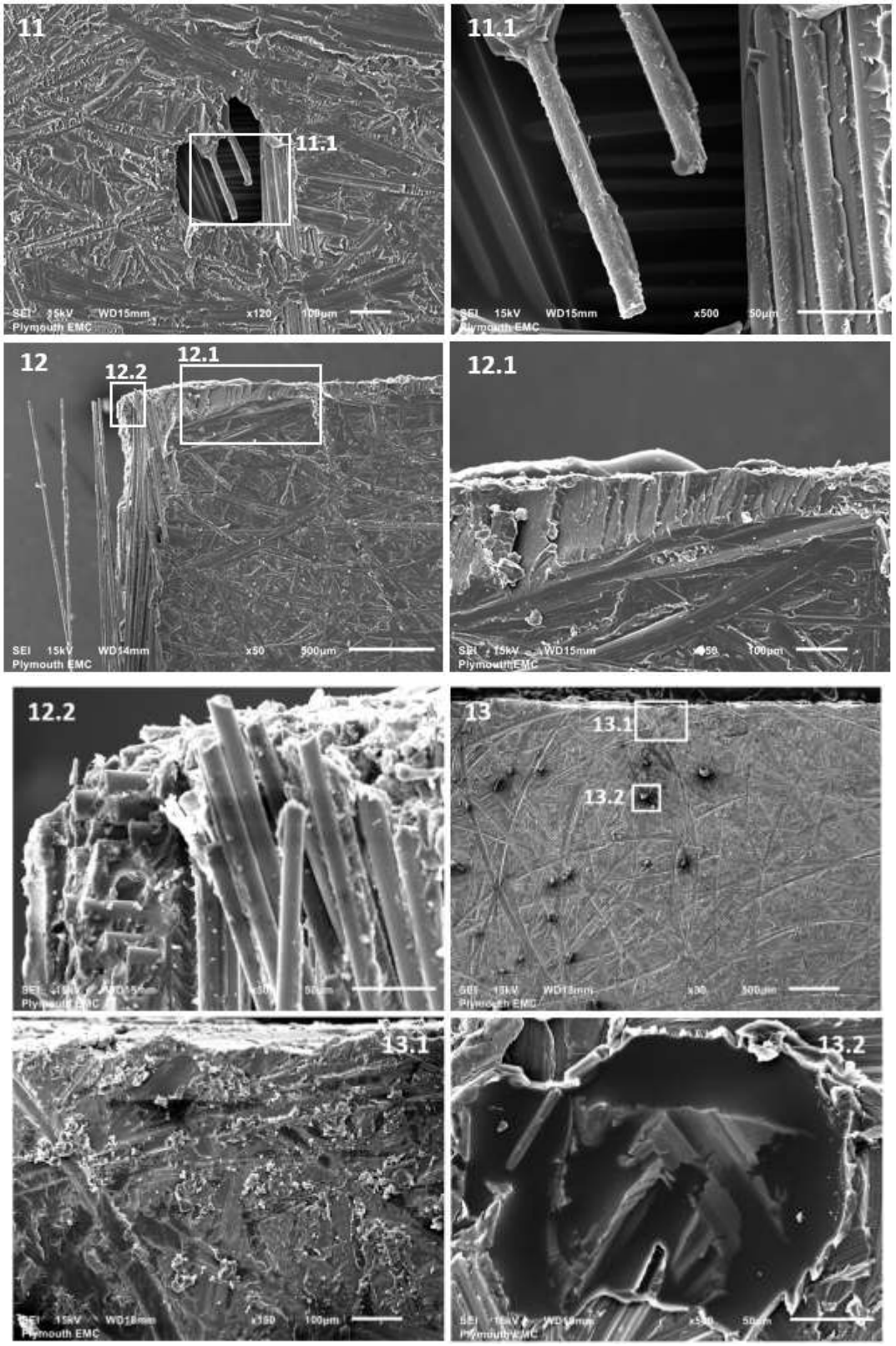

Figure 13: Photograph and micrographs showing the typical fracture surface of a co-cured single-lap joint observed under SEM. (c) fracture surface of GFRP adherend; (d) fracture surface of aluminium adherend.

From the investigations into failure surfaces, there is no substantial evidence of improper surface preparation or adhesion failure. Failure patterns were characteristic of failure within composite-to-metal single-lap joints, and characterised in accordance with BS EN ISO 10365:1995. Adhesively bonded specimens failed by a mixture of cohesive failure with peel. Co-cured specimens failed by a mixture of cohesion, peel and delamination at the first ply layer.

Effect of the bonding process

Figure 14 shows boxplots and mean data points for statistical analysis 1 to 4 showing the effect of the bonding process on the tensile lap-shear strength, by comparing co-cured joints to adhesively bonded ones. The average shear strengths for the co-cured samples with a composite adherend thickness of 20, 15 and 10 plies prepared by mechanical abrasion were 5.16, 2.83 and 2.41 MPa respectively. The corresponding average shear strengths for the adhesively bonded samples were 5.93, 4.37 and 3.09 MPa respectively. Thus, the strength of the adhesively bonded joints were on average 29% higher than the co-cured ones. Statistical analysis was conducted for specimens prepared by mechanical blasting and a composite adherend thickness of 10 plies (see statistical analysis 4). A similar relationship was found, and joint strength of the adhesively bonded joints were approximately 40%

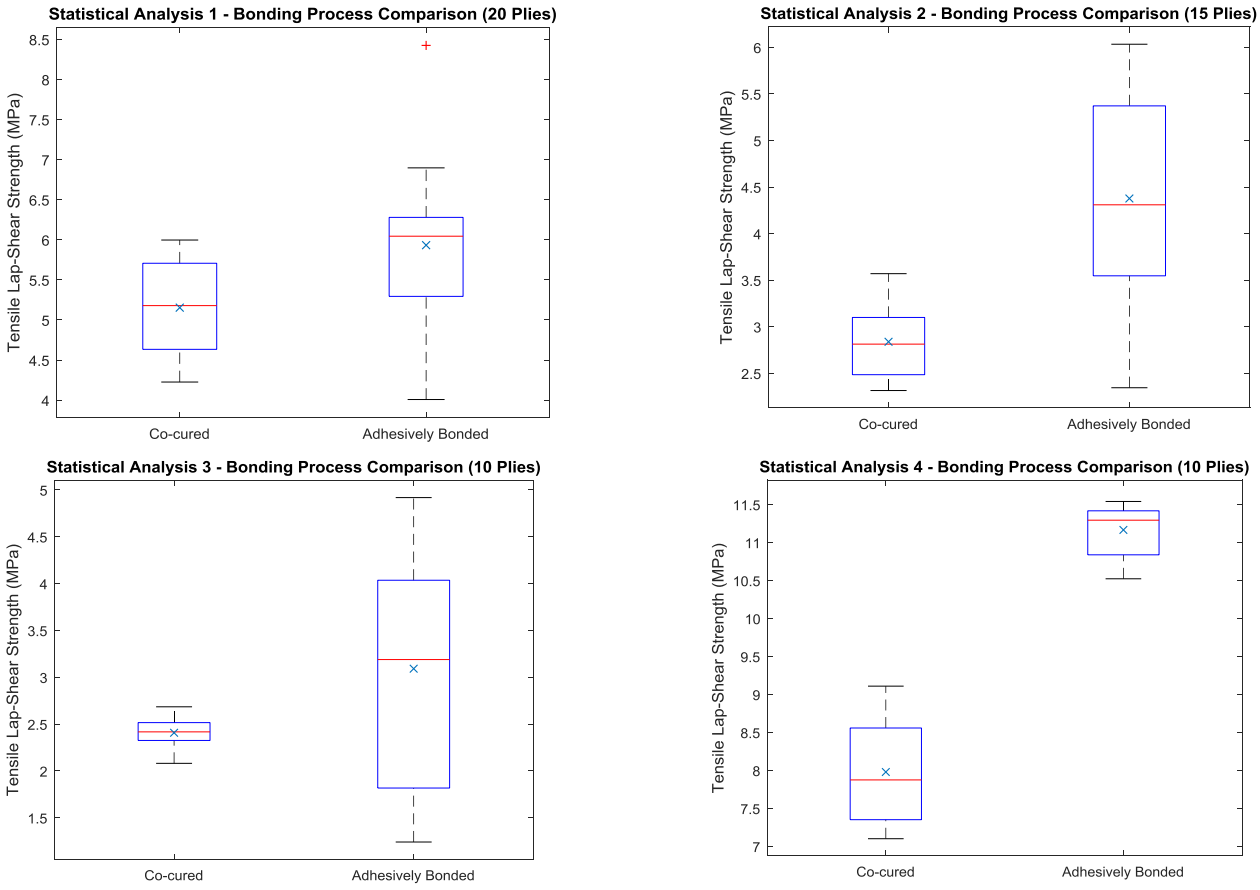

Figure 14: Statistical analysis 1-4 showing bonding process comparisons for a composite adherend thickness of 20, 15 and 10 plies. Statistical analysis 1-3, specimens were prepared by mechanical abrasion. Statistical analysis 4, specimens were prepared by mechanical blasting.

higher than the co-cured ones.

Within statistical analysis 1, 2 and 4, equal variance between the two samples was statistically verified, the corresponding p-values (0.097, 0.0146 and 0.0652) confirm this. Analysis 3 rejected the null hypothesis at the 1% significance level, and variation was assumed unequal.

For statistical analysis 1 and 3, the large *p*-values of 0.1231 and 0.1491 from two-sample testing confirms that joint strengths are similar and the null hypothesis is accepted. For analysis 1, 99% confidence intervals for the difference intercept zero and confirm this result (see Appendix G). For statistical analysis 3 showing unequal variance, nonparametric and log transformation testing was conducted to eliminate any bias from the analysis. These results presented in Appendix G coincide with the two-sample tests, and consequently joint strengths are statistically similar.

Two-sample t-tests for statistical analysis 2 and 4 reject the null hypothesis at the 1% significance level. Consequently, joint strengths are dissimilar. Small p-values of 0.0027 and 5.63E-09 respectively, along with 99% confidence intervals that do not intersect zero (see Appendix G) confirms these results.

The results from each statistical analysis present mixed conclusions. Within analysis 1 and 3, samples prepared by mechanical abrasion and an adherend thickness of 20 plies and 10 plies respectively, there is no significant difference in joint strength between the two bonding processes. Within analysis 2 and 4, prepared by mechanical abrasion and blasting with an adherend thickness of 15 plies and 10 plies respectively, it was shown that joints strengths are significantly different, and adhesively bonded samples were found to be 54% and 40% higher respectively in comparison to co-cured ones. The results of statistical analysis 1 and 3, raises the potential of the co-curing bonding process, as similar joint strengths can be obtained in comparison to adhesive bonding. This result comes with the added advantage of a highly efficient manufacturing process.

Other conclusions can be draw from this analysis. From Figure 14, it is clear that the degree of scatter is greater within the adhesively bonded joints. This observation is mainly due to variation and defects in the manufacturing process such as air cavities as already identified. Other variations include, the application of adhesive and fillet formation at the free ends of the overlap region cannot be precisely controlled. According to Adams and Peppiatt (1974) along with Kwang-Soo Kima (2006), these manufacturing parameters are known to greatly influence joint strength. For the co-cured bonding process, manufacturing parameters such as bonding pressure, adhesive application, fillet formation and bondline thickness can be precisely controlled. Consequently, the range of scatter is significantly lower, which from a manufacturing and failure prediction viewpoint is highly desirable.

Effect of surface preparation

Statistical analysis 5 and 6 presented in Figure 15 shows the effect of surface preparation in terms of joint strength for either bonding process. All comparisons involve a composite adherend thickness of 10 plies. The average joint strengths for the adhesively bonded samples prepared by mechanical blasting and abrasion were 11.16 and 3.09 MPa respectively, resulting in a 262% increase in joint strength with adoption of mechanical blasting over abrasion.

For the co-cured joints, similar results were found. The average shear strengths of the joints prepared by mechanical blasting and abrasion were 7.97 and 2.41 MPa respectively, with a corresponding increase in joint strength of approximately 231%.

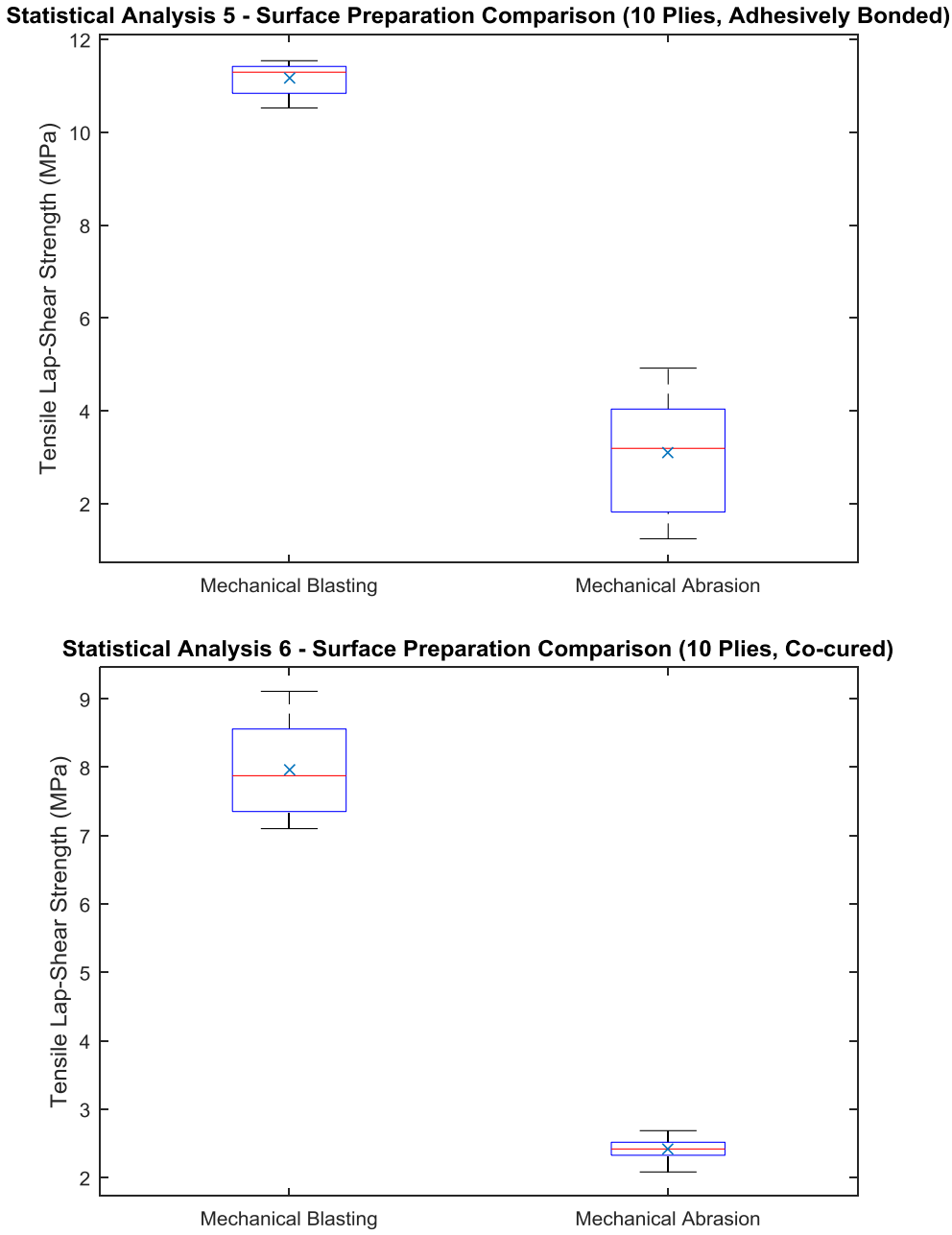

Figure 15: Statistical analysis 5 and 6, showing surface preparation comparisons for a composite adherend thickness of 10 plies. Statistical analysis 5 specimens were manufactured by adhesive bonding. Statistical analysis 6 specimens were manufactured by co-curing.

Statistical analysis was used to validate the initial visual observations made. For each analysis, both tests rejected the null hypothesis for equal variance at the 1% significance level. Small p-values (1.00E-03 and 1.70E-03) confirm this, and unequal variance was assumed. Unequal variance two-sample t-tests were conducted and

both analyses rejected the null hypothesis. This indicates that the differences in joint strengths are significant. The fact that the corresponding p-values (3.08E-09 and 3.19E-08) are small, and 99% confidence intervals (see Appendix G) do not intersect zero confirms this result.

As a consequence of unequal variance, nonparametric and log transformation testing were conducted for each analysis and the same conclusions were found (see Appendix G). The results from statistical analysis 5 and 6 indicate that for both bonding processes, joint strength is greatly influenced by the surface pre-treatment process. The adoption of mechanical blasting over abrasion has a greater effect in the adhesively bonded joints as the degree of scatter is significantly reduced, and larger increments in joint strength are obtained. For the co-cured specimens, similar results were found but to a lesser extent.

Effect of surface roughness

Previous studies (Pereira *et al.* 2010; Tzetzis, 2012) report that surface roughness greatly influences joint strength. Therefore, it is important to investigate the surface roughness of the aluminium adherend for each surface pre-treatment process.

Surface roughness measurements were conducted using an Olympus LEXT OLS3000 confocal laser scanning microscope (CLSM) (Olympus Corporation , 2003) with a Table Stable (TS-150) anti-vibration mounting table (JRS Scientific Instruments, 2016). For each preparation process, average areal surface roughness parameters were obtained by measuring the surface roughness over five separate areas on each sample as shown in Appendix C.

Figure 16 shows the relationship between the average areal surface roughness (SR_a) for the two surface pre-treatment processes examined in this study. SR_a is the arithmetic mean value of the areal roughness depths of five samples.

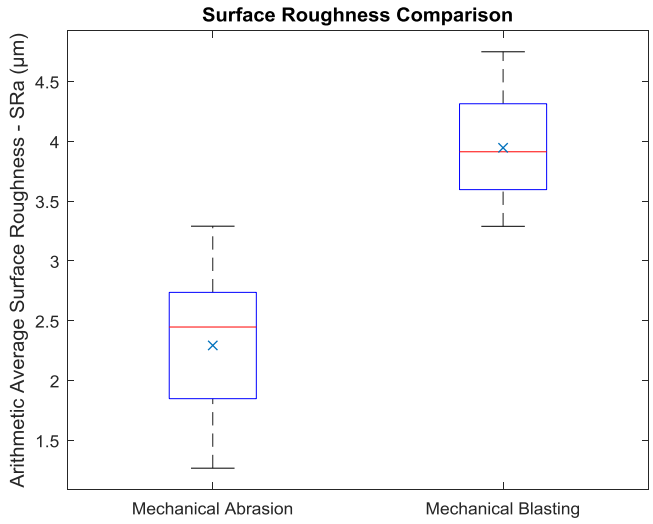

Figure 16: Relationship between the arithmetic average surface roughness and the surface pre-treatment process for the 1050 H19 series aluminium alloy.

Results indicate that the average surface roughness of the mechanical blasted adherends is greater than those prepared by mechanical abrasion. Figures 17 and 18 illustrate a typical two-dimensional and three-dimensional image for each pre-treatment process. Notice how the images presented clearly depict how uniform scarification is when the blasting process is used. Between the two, the surface morphologies are noticeably different, and different physical features are present. For example, within the abraded surface (Figure 18, a) there are regions of long striations where the surface is polished and then sub regions where scarification similar to the blasted specimen (Figure 18, b) occurs.

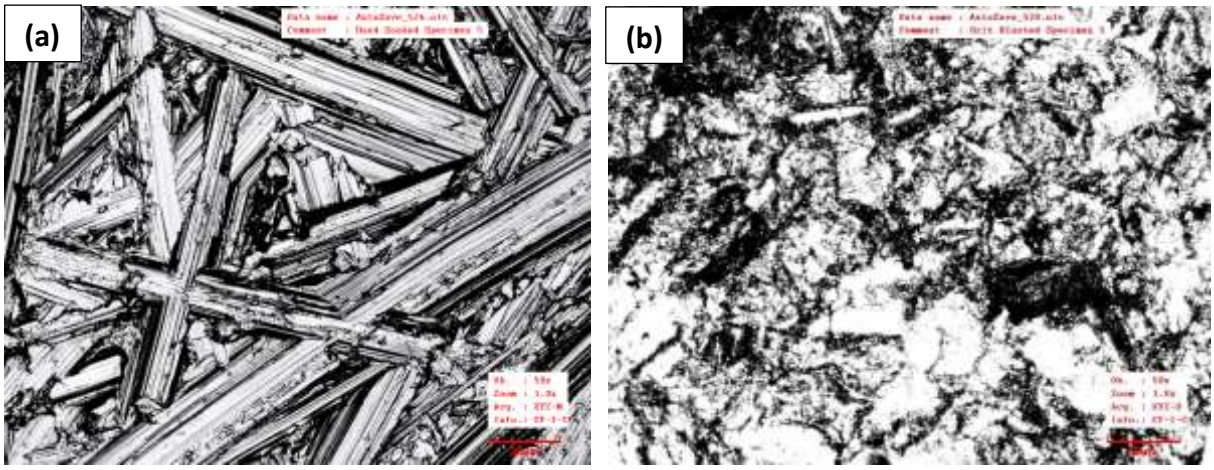

Figure 17: Typical 2D micrographs of 1050 H19 series aluminium alloy prepared by; (a) **mechanical abrasion and (b) mechanical blasting.**

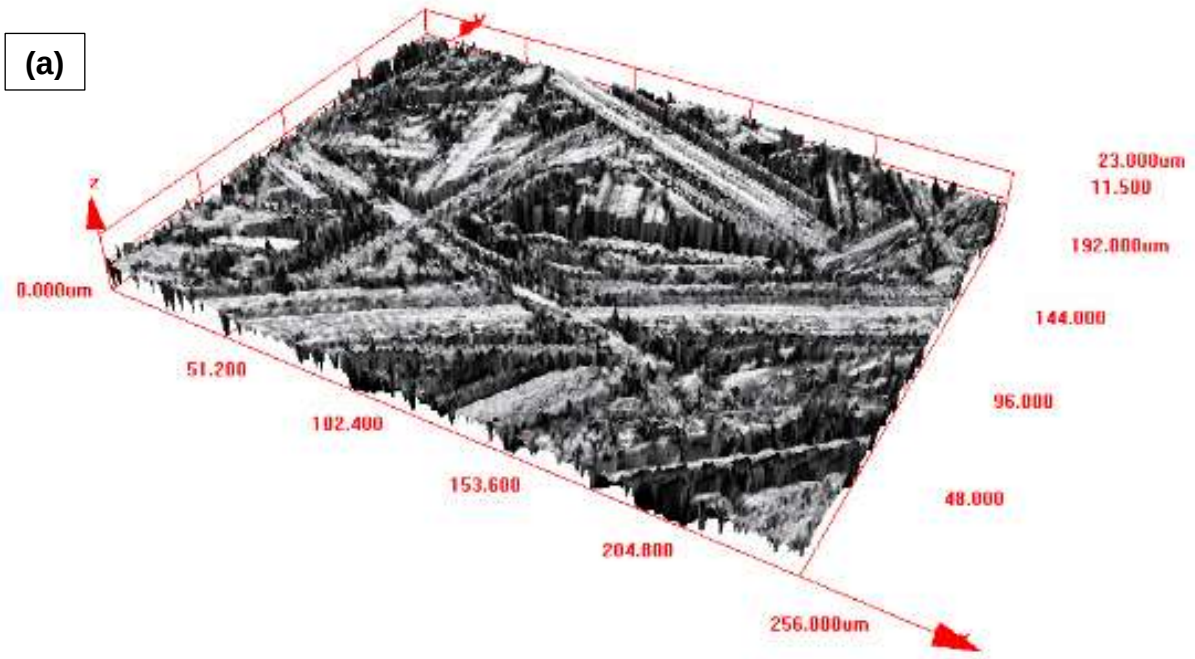

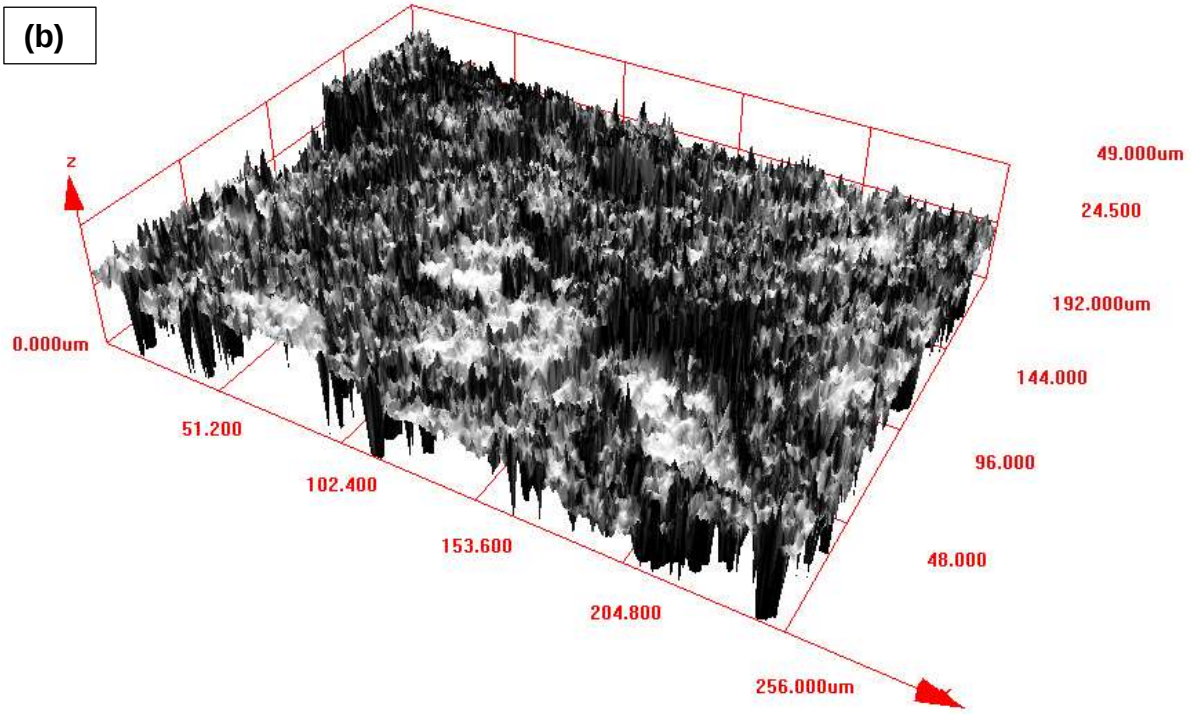

Figure 18: Typical 3D micrographs of 1050 H19 series aluminium alloy prepared by; (a) mechanical abrasion and (b) mechanical blasting (note y-direction scale differences).

The results of this analysis presented in Figure 19 indicate that the highest surface roughness attained from the mechanically blasted adherends, corresponds to the most effective adhesion. Consequently, specimens prepared by mechanical blasting achieve higher joint strengths. This was not expected. According to Kwang-Soo Kima (2006), Pereira *et al*. (2010) and Tzetzis (2012), a lower surface roughness promotes a smaller angle of contact, better wettability and higher joint strengths. The results of this study contradict these findings. However, the fact that two difference surface pre-treatment processes were selected must be carefully considered, as the surface roughness relationship for different grit sizing has not been considered in this study.

Besides this, results of this analysis clearly indicate that for the two surface pre-treatment processes studied, a higher surface roughness corresponds to greater joint strengths. In fact, an increase in joint strength of 262% and 231% can be obtained by mechanical blasting over abrasion for either bonding process. From the results studied so far, surface pre-treatment and roughness have the greatest influence on joint strength within single-lap joints

.

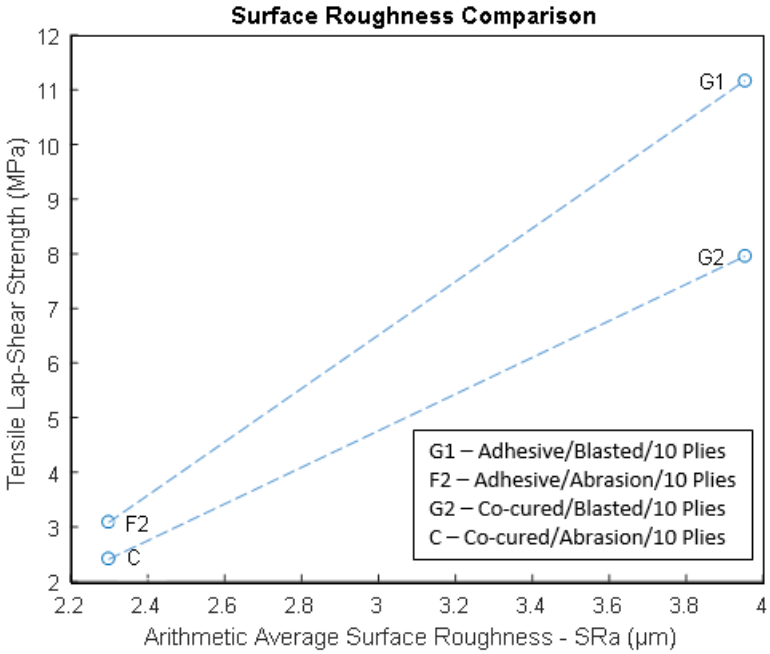

Figure 19: Relationship between the arithmetic average surface roughness on the tensile lap-shear strength for co-cured and adhesively bonded test specimens prepared by mechanical blasting and mechanical abrasion.

Effect of adherend thickness

Figure 20 shows the effect of composite adherend thickness on the tensile lap-shear strength for the two bonding processes examined in this study. As expected, for both bonding techniques higher joint strengths are obtained with an increase in adherend thickness, since peak stresses at the ends of the overlap region are reduced which promotes more uniform stress distribution.

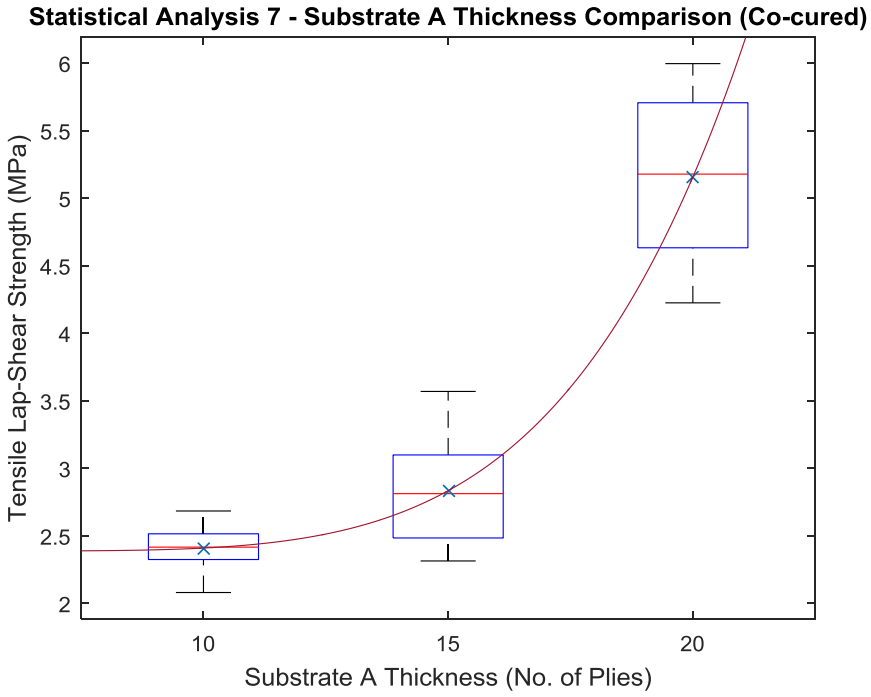

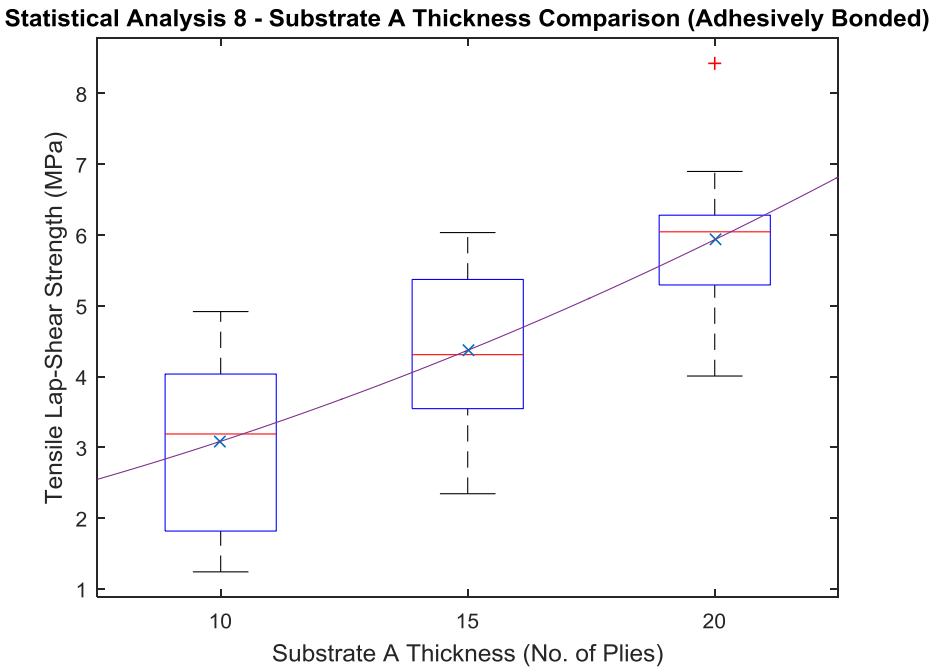

Figure 20: Statistical analysis 7 and 8 showing the effect of composite adherend thickness on the tensile lap-shear strength for; (a) co-cured and (b) adhesively bonded specimens.

For both bonding processes, three-sample statistical hypothesis testing was conducted and it was verified that increasing the adherend thickness results in a significant increase in joint strength. The corresponding small p-values of 7.7250e-11 and 1.0206e-04 from one-way ANOVA confirm this.

For the co-cured joints (statistical analysis 7), multiple comparison mean tests presented in Appendix H confirms that there is a significant increase in joint strength when adherend thickness is increased from 10 or 15 plies to 20 plies. Because the corresponding *p*-values (1.1496e-09 and 4.3976e-09, respectively) are small, and confidence intervals do not include zero, the differences in joint strength are statistically significant. Consequently, an increase in joint strength of 114% and 105% is found. Results presented in Figure 20 indicate that strength increases exponentially when adherend thickness is increased. This is advantageous, as substantial increments in joint strength can be achieved with relatively small increments in composite adherend thickness, but up to a limiting value. In another study, Reis *et al.* (2011) reports that for higher values of bending stiffness, the failure load tends to stabilise and become independent of this parameter.

For the adhesively bonded joints (statistical analysis 8), results presented in Appendix H confirm that there is a significant increase in strength when adherend thickness is increased from 10 or 15 plies to 20 plies. As corresponding *p*-values (6.3253e-05 and 0.0239, respectively) are small, and confidence intervals do not include zero, the differences in joint strength are statistically significant.

Consequently, an increase in joint strength of 92% and 36% is obtained. Results, show that the general trend is a linear relationship and consequently, increasing the adherend thickness is less effective within the adhesively bonded joints. As a result, large increments in adherend thickness are required for any substantial increase in joint strength.

Within either bonding process, for comparisons involving an adherend thickness of 10 and 15 plies, it is found that the differences in strength are not statistically significant. 99% confidence intervals intercept zero, and large corresponding *p*-values of 0.1685 and 0.0711 confirm this result.

From the results, it was also found that the degree of scatter within the adhesively bonded samples is equal across all three samples. The large p-value of 0.9048 from Bartlett's multiple-sample test for equal variance confirms this. This was not the case for the co-cured joints, as clearly depicted in Figure 20, and the variance of the samples increased with adherend thickness. Greater variance is observed since with thicker adherends comes greater rigidity. Consequently, the interlaminar shear strength of the composite adherend becomes the limiting factor in the failure of the joint, as evidenced in Section 6.1. But also notice in Appendix D how there are small fluctuations in load as delamination occurs prior to failure.

The results of this analysis, agree with previous studies (Seong *et al.* 2008; Pereira *et al.* 2010; Reis *et al.* 2011; Pinto *et al.* 2014) and can be explained by an increase in joint rigidity. Although an increase in adherend thickness results in an increase in the bending moment. Since the bending stiffness of the adherend is proportional to the cubic of its thickness, thicker adherends gives higher joints strengths regardless of the bending moment increase due to loading eccentricity. Consequently, rotational angles are reduced (Pereira *et al*. 2010), peel stresses at the ends of the overlap region are minimised, more uniform stress distribution occurs, and the adhesive is able to develop its full resistance capacity.

Effect of bondline thickness

Results for statistical analysis 9 to 11 presented in Figure 21 show mixed conclusions. Analysis 9 shows that the general trend is that the tensile lap-shear strength increases with a corresponding decrease in adhesive layer thickness, which coincides with the literature reported in previous studies (Bigwood & Crocombe, 1990; Da Silva *et al.* 2006; Kwang-Soo Kima, 2006; Kahraman *et al.* 2008; Lee *et al.* 2009). Within analysis 10, although the general trend is similar to that observed in analysis 9, it was statistically verified that the difference in joint strength between the three parameters are insignificant. Hence joint strengths are similar and we cannot reject the null hypothesis. For each comparison, 99% confidence intervals for the difference intercept zero and the large *p*-values presented in Appendix H confirm this.

From analysis 11 no clear correlation between bondline thickness and joint strength can be made. Statistical analysis was conducted, and results confirm that the differences in joint strengths are insignificant.

For each comparison, 99% confidence intervals for the difference intercept zero, and corresponding *p*-values (0.3325, 0.7158 and 0.0841) are large. Results from analysis 10 and 11 provide an indication that an adherend thickness of 10 and 15 plies provides insufficient rigidity of the joint in order to test the full resistance capacity of

the adhesive, and consequently the effects of bondline thickness are negligible or ignored in the analysis.

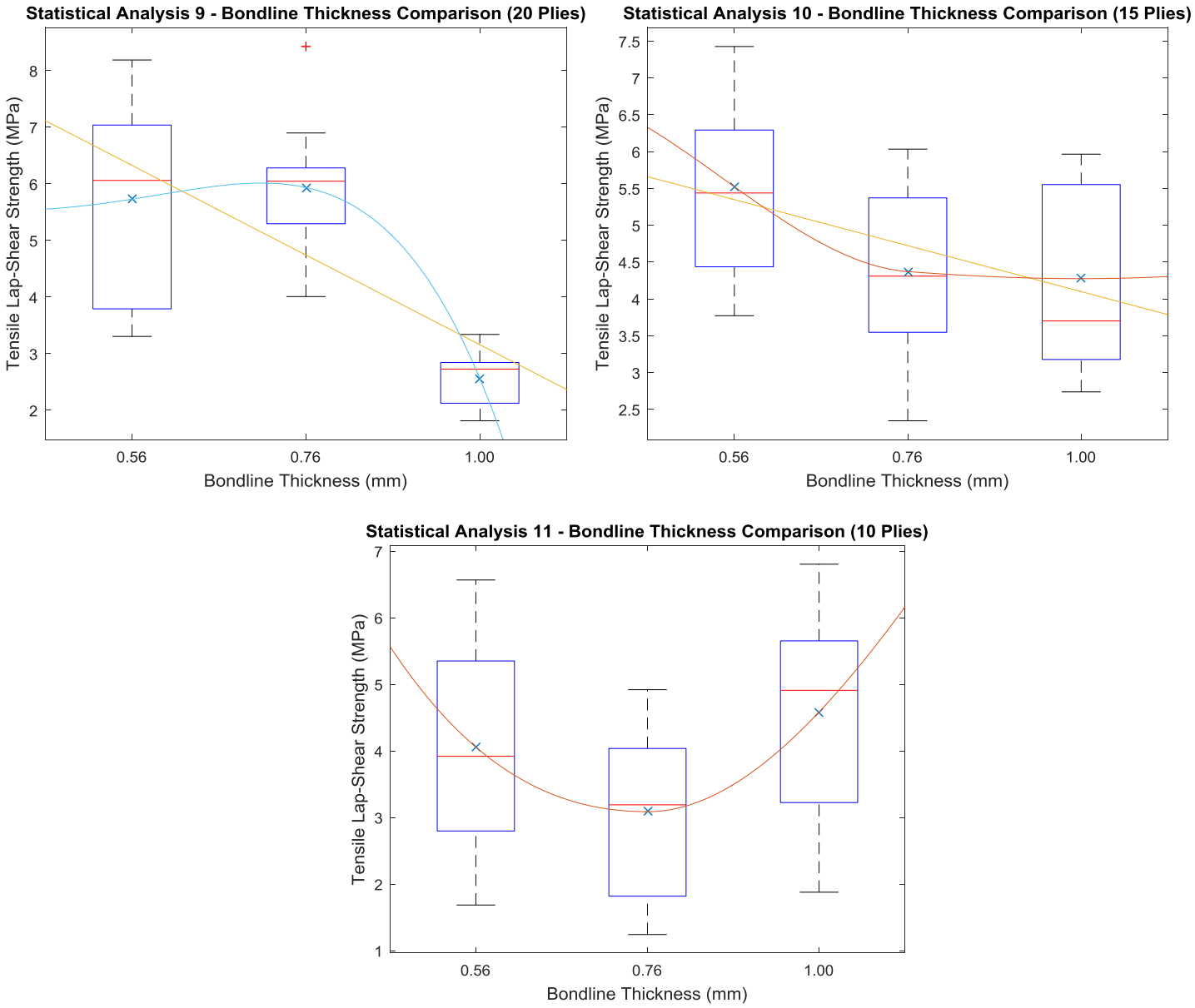

Figure 21: Statistical analysis 9-10, showing the effect of bondline thickness on the tensile lap-shear strength for the adhesively bonded test specimens with a composite adherend thickness of 20, 15 and 10 plies respectively.

This observation is consistent with the results found in Section 6.5, where no clear relationship for an adherend thickness of 10 and 15 plies was distinguishable.

For statistical analysis 10 and 11, it is worth noting that Bartlett's multiple-sample test for equal variances accepts the null hypothesis that the variances are equal across all three samples; meaning we can accept the results with full confidence. Bartlett's test for statistical analysis 9 however, rejects the null hypothesis, in favour of the alternative hypothesis that at least one sample has a different variance. The low p-value (0.0601) confirms this result, and consequently overestimates during the mean comparisons must be carefully considered.

The results from statistical analysis 9 indicate that the differences between sample means are significant, as we would expect from the published literature. Mean comparison tests confirms that both comparisons involving the 1mm bondline thickness are statistically different. Because the corresponding *p*-values (6.1965e-04 and 4.4682e-05, respectively) are small, and confidence intervals do not include zero, the differences in joint strength are significant. From this analysis, an increase in joint strength of 132% and 124% is obtained when bondline thickness is reduced from 1mm to 0.76mm and 0.56mm respectively. For thinner bondlines, according to Bigwood and Crocombe (1990), higher joint strengths are obtained as yielding in the adhesive occurs at lower loads and stresses are less distributed in the overlap. Consequently, sufficient elastic reserve can be obtained in order to sustain further loading.

Other conclusions can be draw from this analysis. Mean comparison testing for statistical analysis 9, confirms that the difference in strength between a bondline thickness of 0.56mm and 0.76mm is not significant. This indicates that any further reductions in bondline thickness will not greatly influence joint strength. According to the published literature, this is not the case, but as already mentioned, there is some uncertainty in these results due to unequal variance. Furthermore, only a narrow range of bondline thicknesses has been studied and further studies outside this range of variables is required in order to capture the full effect.

Manufacturing process comparison

Appendix I shows a standard work combination table for a single operator and the two bonding processes examined in this study, results from Appendix I are presented graphically in Figure 22. From a manufacturing perspective, it is shown within Figure 22 how efficient the co-curing process is in comparison to adhesive bonding. To fabricate twenty co-cured specimens presented in this study, overall cycle time is reduced by 30%, from 50 to 35 hours in comparison to the adhesive bonding process. In adhesive bonding, the majority of the waiting time (38.5 hours) arises due to the requirement to fabricate and cure the composite part prior to adhesive bonding. In co-curing, the operator can achieve these two processes (fabrication of the composite part and bonding) simultaneously, additionally there is no requirement to control adhesive layer thickness or fillets, and hence the working sequence is simplified.

In addition to the manufacturing time and cost improvements, it is clear from Figure 23 that the quality and consistency (in terms of degree of scatter) of the co-cured specimens (A, B, and C) is better than the adhesively bonded ones (D2, E2 and F2), with the exception for G1 and G2 prepared by mechanical blasting.

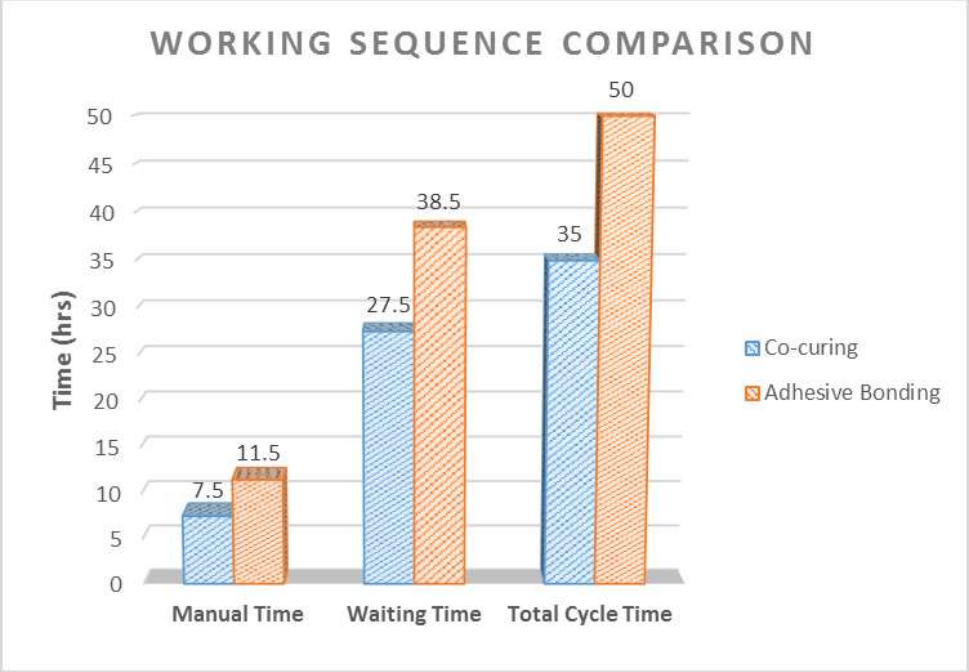

Figure 22: Graphical representation of a standard work combination table for each bonding process presented in Appendix I.

From a lifecycle analysis or failure prediction standpoint, the ability to predict joint strength from a manufacturing process that is under statistical control is highly advantageous. Mean ($\bar{x}$) statistical process control (SPC) charts for each manufacturing process are presented in Appendix J and validate this statement. From these charts it is shown that all co-cured samples remain within ± 2 standard deviations from the mean. Within the adhesively bonded samples, some specimens deviate outside this tolerance range, but are generally under statistical control.

From a manufacturing viewpoint, it is shown below (Figure 24) how the co-curing bonding process can be adopted in industrial applications over adhesive bonding. By simply modifying adherend thickness, it is shown how the strength of the co-cured joints matches, or even better, exceeds the strength of the adhesively bonded ones. For example, in comparing samples A and E2 which were prepared by mechanical abrasion, increasing the thickness of the composite adherend from 15 to 20 plies within the co-cured specimen will yield an 18% increase in joint strength over a 15 ply adhesively bonded joint. The use of additional material is not a primary concern since the savings obtained in terms of manufacturing cycle times, better quality control and reliability by far outweigh the cost and weight associated with additional material. Even with additional material the mass of the structure is likely to be lighter than traditional joining methods.

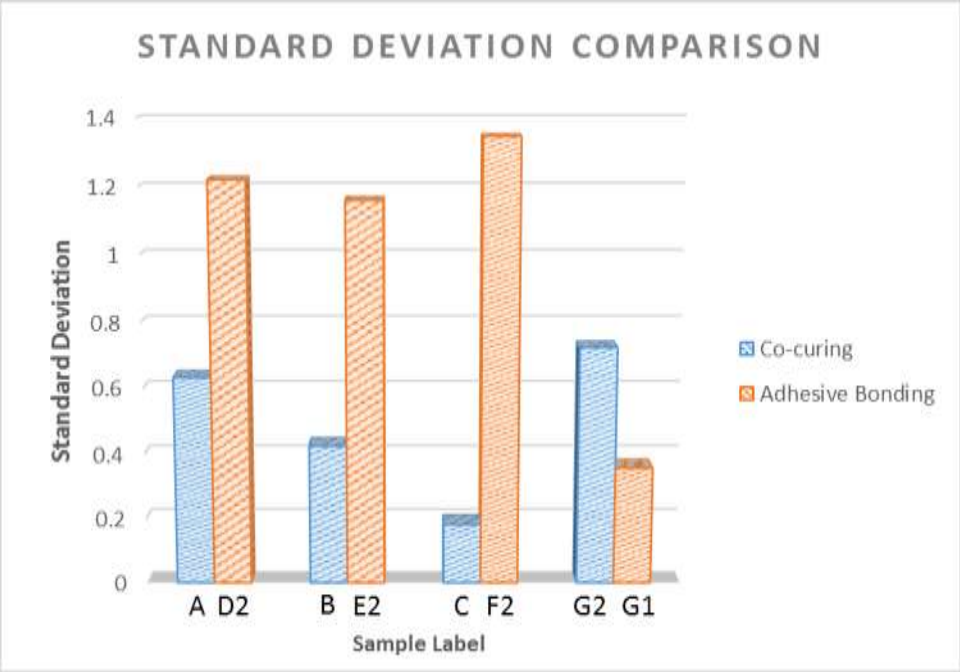

Figure 23: Standard deviation comparison, showing the measure of spread for each bonding process.

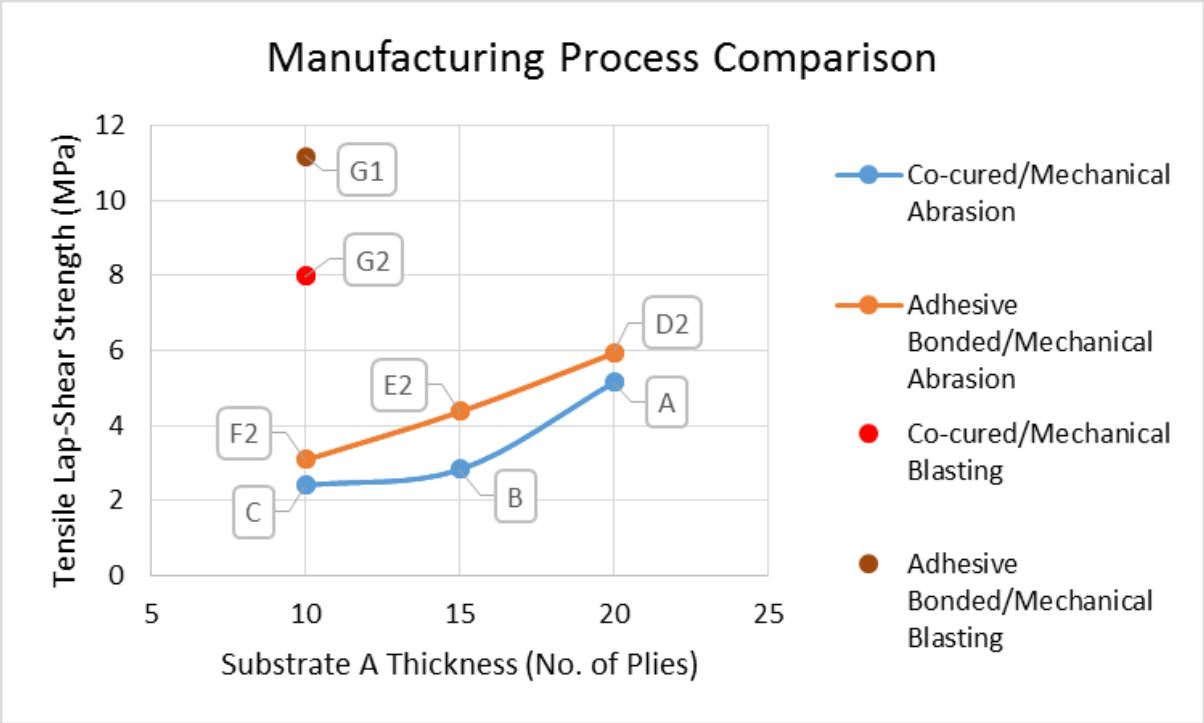

Figure 24: Manufacturing process comparison.

Results of this analysis, also picture how powerful surface preparation is during the manufacturing process. By simply adopting a better surface pre-treatment process, it is clear how the strength of the co-cured joint (sample G2) exceeds the strength of the adhesively bonded ones (D2, E2 and F2) prepared by mechanical abrasion which is typical of many industrial applications (Wahab, 2015). This manufacturing parameter provides one other alternative to increasing the application of co-curing in industry. Unlike the previous comparison, one important aspect is that this improvement comes with no increase in the use of raw materials. In fact, simply through better surface preparation, reductions in the use of raw materials and further weight savings are attainable. Since, a typical 20 ply adhesively bonded joint (sample D2) prepared by mechanical abrasion, can be replaced by a co-cured joint with a composite adherend thickness of 10 plies (sample G2). This corresponds to approximately a 50% reduction in the weight of the composite part, with the added advantage of additional strength (34% increase) and lower manufacturing costs. The results of this analysis clarifies how powerful the surface pre-treatment process is and the effect of composite adherend thickness. This allows engineers to tailor the co-curing process so that from a manufacturing perspective it is superior over adhesive bonding and traditional joining methods.

Conclusions

In this study, GFRP-to-aluminium single-lap joints were manufactured and tested under static tensile loading. The influence of four different manufacturing parameters (bonding process, adherend thickness, bondline thickness and surface preparation) on the tensile lap-shear strength were studied. A full manufacturing analysis was conducted and results were verified by statistical hypothesis testing. Numerical studies were conducted to investigate the stress distributions along the overlap region which could not be obtained experimentally. From the experimental and numerical investigations, the following conclusions were drawn:

[1] The co-cured joining method was examined, which is a relatively new manufacturing process utilising excess resin extracted from the composite material during the bonding process. From a manufacturing perspective, it was shown that this joining method is highly efficient and manufacturing parameters such as bonding pressure, adhesive application, fillet formation and bondline thickness can be precisely controlled.

[2] Results from the FEA indicate that shear stresses along the overlap region are non-uniformly distributed and peak stresses decrease with a corresponding increase in adherend thickness. Throughout the co-cured joints, increasing the thickness of a single adherend results in peel and shear stresses concentrated at one end of the joint.

[3] Adhesively bonded joints failed by a mixture of cohesive failure with peel. For the co-cured joints, the failure mechanism was cohesive failure by delamination at the first ply layer. It was found that the interlaminar shear strength of the composite adherend becomes the limiting factor in the failure of the joint.

[4] The strength of the adhesively bonded joints prepared by mechanical abrasion were on average 29% higher than the co-cured ones. Joint strength of the adhesively bonded joints prepared by mechanical blasting were approximately 40% higher than the co-cured ones.

[5] Joint strength is greatly influenced by the surface pre-treatment process. An increase in joint strength of 262% and 231% for the adhesively bonded and co-cured joints was found with adoption of mechanical blasting over abrasion. Results indicate that the highest surface roughness attained from the mechanically blasted adherends, corresponds to the most effective adhesion.

[6] For both bonding processes higher joint strengths are obtained with an increase in adherend thickness. For the co-cured joints, strength increases exponentially when adherend thickness is increased. For the adhesively bonded joints the general trend is a linear relationship.

[7] For the effect of bondline thickness, the general trend is that the tensile lap-shear strength increases with a corresponding decrease in adhesive layer thickness.

References

Adams, R. D., 2005. *Adhesive bonding : science, technology and applications.* 1st ed. Cambridge: Woodhead Publishing.

Adams, R. D. & Peppiatt, N. A., 1974. Stress analysis of adhesive-bonded lap joints. *The Journal of Strain Analysis for Engineering Design,* 9(3), pp. 185-196.

Adhesives Toolkit, 2015. *Stress Analysis Toolkit.* [Online]
Available at: http://www.adhesivestoolkit.com/Toolkits/StressAnalysis/Material.xtp
[Accessed 8 November 2015].

Asgari Mehrabadi, F. & Ganguli, R., 2012. Experimental and Numerical Failure Analysis of Adhesive Composite Joints. *International Journal of Aerospace Engineering,* 12(12), pp. 0-10.

ASTM International, 2014. *ASTM D5868 - 01(2014), Standard Test Method for Lap Shear Adhesion for Fiber Reinforced Plastic (FRP) Bonding.* West Conshohocken, Pa, USA: ASTM.

Autodesk Inc., 2016. *Helius Composite.* [Online]
Available at: http://www.autodesk.co.uk/products/helius-composite/overview

Baker, A. A., Rose, L. R. F. & Jones, R., 2002. *Advances in the bonded composite repair of metallic aircraft structure.* 1st ed. Boston: Elsevier.

Bigwood, D. & Crocombe, A., 1989. Elastic analysis and engineering design formulae for bonded joints. *Int. J. Adhesion Adhesives,* 9(1), pp. 229-242.

Bigwood, D. & Crocombe, A., 1990. Non-linear adhesive bonded joint design analyses. *Int. J. Adhesion Adhesives,* Volume 10, pp. 31-41.

British Standards Institution, 1995. *BS EN ISO 10365:1995 Adhesives. Designation of main failure patterns.* London: BSI.

British Standards Institution, 2003. *BS EN 13887:2003 Structural adhesives. Guidelines for surface preparation of metals and plastics prior to adhesive bonding.* London: BSI.

Broughton, B. & Gower, M., 2001. *Performance of Adhesive Joints.* [Online]
Available at: http://tinyurl.com/3xouywf
[Accessed 28 November 2015].

Campbell, F. C., 2004. *Manfacturing processes for advanced composites.* 1 ed. New York: Elsevier.

Cheng, S., Chen, D. & Shi, Y., 1991. Analysis of Adhesive-Bonded Joints with Nonidentical Adherends. *Journal of Engineering Mechanics,* 118(9), pp. 1962-1973.

Da Silva, L. F. M. et al., 2006. Effect of Adhesive Type and Thickness on the Lap Shear Strength. *The Journal of Adhesion,* 82(11), pp. 1091-1115.

Dassault Systèmes SolidWorks Corp., 2015. *SolidWorks 2015.* s.l.:s.n.

de Morais, A., Pereira, A., Teixeira, J. & Cavaleiro, N., 2007. Strength of epoxy adhesive-bonded stainless-steel joints. *International Journal of Adhesion and Adhesives,* 27(8), pp. 679-686.

Goland, M. & Reissner, E., 1944. The stresses in cemented joints. *J Applied Mechanics,* Volume 66, pp. 17-27.

GRANTA DESIGN, 2015. *CES EduPack.* s.l.:s.n.

Gurit , 2016. *SPABOND 340LV - EPOXY ADHESIVE SYSTEM.* [Online]
Available at: http://www.gurit.com/files/documents/spabond-340lvv14pdf.pdf
[Accessed 10 April 2016].

Hart-Smith, L., 1973. Adhesive bonded single-lap joints - technical report. *NASA report CR-112236.*

Hudson, B., 2014. *Rewind...April 21-26 1988: Aircraft drama was big news.* [Online]
Available at: http://tinyurl.com/owge7xs
[Accessed 22 November 2015].

Instron, 2016. *5500 Series.* Buckinghamshire: s.n.

JEOL , 2016. *JSM-6610 Series Scanning Electron Microscope.* [Online]
Available at: http://www.jeol.co.jp/en/products/detail/JSM-6610series.html
[Accessed 14 April 2016].

JRS Scientific Instruments, 2016. *TS-150.* [Online]
Available at: http://www.tablestable.com/uploads/ckeditor/TS-150/Manual%20TS-150_%20TS-140_%20TS-300LP.pdf
[Accessed 11 April 2016].

Kahraman, R., Sunar, M. & Yilbas, B., 2008. Influence of adhesive thickness and filler content on the mechanical performance of aluminum single-lap joints bonded with aluminum powder filled epoxy adhesive. *Journal of Materials Processing Tech.,* 205(1), pp. 183-189.

Kinloch, A. J., 1983. *Durability of structural adhesives.* London: Applied Science.

Kinloch, A. J., 1987. *Adhesion and adhesives : science and technology.* London: Chapman and Hall.

Kwang-Soo Kima, J.-S. Y. Y.-M. Y. C.-G. K., 2006. Failure mode and strength of uni-directional composite single lap bonded joints with different bonding methods. *Composite Structures,* 72(4), p. 477–485.

Lee, H., Pyo, S. & Kim, B., 2009. On joint strengths, peel stresses and failure modes in adhesively bonded double-strap and supported single-lap GFRP joints. *Composite Structures,* 87(1), pp. 44-54.

Matsuzaki, R., Shibata, M. & Todoroki, A., 2008a. Improving performance of GFRP/aluminum single lap joints using bolted/co-cured hybrid method. *Composites Part A,* 39(2), pp. 154-163.

Matsuzaki, R., Shibata, M. & Todoroki, A., 2008b. Reinforcing an aluminum/GFRP co-cured single lap joint using inter-adherend fiber. *Composites Part A,* 39(5), pp. 786-795.

Mazumdar, S. K., 2001. *Composites manufacturing : materials, product, and process engineering.* London: CRC Press.

Olympus Corporation , 2003. *Olympus LEXT OLS3000 Confocal Laser Scanning Microscope.* s.l.:s.n.

OLYMPUS CORPORATION, 2016. *DELTA Professional.* [Online]
Available at: http://www.olympus-ims.com/en/xrf-xrd/delta-handheld/delta-prof/#!cms[tab]=%2Fxrf-xrd%2Fdelta-handheld%2Fdelta-prof%2Foverview
[Accessed 12 April 2016].

O'Mahoney, D. et al., 2013. Taguchi analysis of bonded composite single-lap joints using a combined interface–adhesive damage model. *International Journal of Adhesion and Adhesives,* Volume 40, pp. 168-178 .

Pereira, A., Ferreira, J., Antunes, F. & Bártolo, P., 2010. Analysis of manufacturing parameters on the shear strength of aluminium adhesive single-lap joints. *Journal of Materials Processing Tech.,* 210(4), pp. 610-617 .

Pinto, A. M. G., Campilho, R. D. S. G., Mendes, I. R. & Baptista, A. P. M., 2014. Numerical and Experimental Analysis of Balanced and Unbalanced Adhesive Single-Lap Joints Between Aluminium Adherends. *The Journal of Adhesion,* 90(1), pp. 89-103.

QuinII, J. G. & MarinucciII, G., 2012. Polyurethane structural adhesives applied in automotive composite joints. *Materials Research,* 15(3), pp. 434-439.

Quorum Technologies, 2016. *K550X Sputter Coater Instruction Manual.* [Online]
Available at: https://www.quorumtech.com/ assets /pdf/Manuals%5CK550X-Manual-Iss5-NEW-LOGO.pdf
[Accessed 14 April 2016].

Reis, P., Ferreira, J. & Antunes, F., 2011. Effect of adherend's rigidity on the shear strength of single lap adhesive joints. *International Journal of Adhesion and Adhesives,* 31(4), pp. 193-201.

Seong, M.-S.et al., 2008. A parametric study on the failure of bonded single-lap joints of carbon composite and aluminum. *Composite Structures,* 86(1), pp. 135-145.

Shin, K. C. & Lee, J. J., 2000. Tensile load-bearing capacity of co-cured double lap joints. *Journal of Adhesion Science and Technology,* 14(12), pp. 1539-1556.

Shin, K. C., Lim, J. O. & Lee, J. J., 2003. The manufacturing process of co-cured single and double lap joints and evaluation of the load-bearing capacities of co-cured joints. *Journal of Materials Processing Tech.,* 138(1), pp. 89-96.

Sicomin Epoxy Systems, 2016. *Epoxy Systems - Injection.* [Online]
Available at: http://www.sicomin.com/datasheets/product-pdf94.pdf
[Accessed 10 April 2016].

Song, M.-G.et al., 2010. Effect of manufacturing methods on the shear strength of composite single-lap bonded joints. *Composite Structures,* 92(9), pp. 2194-2202.

The MathWorks, Inc., 2016. *MATLAB R2015b.* [Online]
Available at: http://uk.mathworks.com/products/matlab/
[Accessed 12 April 2016].

Tzetzis, D., 2012. Characterisation of GFRP surfaces amenable for bonding and their effect on the strength of co-cured vacuum resin infused single lap joints. *Journal of Adhesion Science and Technology,* 26(24), pp. 2683-2707.

Vogelesang, L. & Vlot, A., 2000. Development of fibre metal laminates for advanced aerospace structures. *Journal of Materials Processing Tech,* 103(1), pp. 1-5.

Volkersen, O., 1938. Rivet strength distribution in tensile-stressed rivet joints with constant cross-section. *Luftfahrtforschung,* Volume 15, pp. 41-47.

Wahab, M. A., 2015. *Joining Composites with Adhesives : Theory and Applications.* 1st ed. Lancaster : DEStech Publications, Inc.

Zhao, B., Lu, Z.-H. & Lu, Y.-N., 2011. Closed-form solutions for elastic stress–strain analysis in unbalanced adhesive single-lap joints considering adherend deformations and bond thickness. *International Journal of Adhesion and Adhesives,* 31(6), pp. 434-445.

Appendices for this work can be retrieved within the Supplementary Files folder which is located in the Reading Tools menu adjacent to this PDF window.